Supplementary Material

Molecular engineering of dendritic luminogens with thermally activated delayed fluorescence and aggregation-induced emission characteristics for efficient solution-processed nondoped OLEDs

*Fulong Ma[a], Xinxin Zhao[a], Hefang Ji[a], Dongdong Zhang[a], Kamran Hasrat[a], Zhengjian Qi[a]**

[a]Jiangsu Province Hi-Tech Key Laboratory for Biomedical Research, School of Chemistry and Chemical Engineering, Southeast University, Nanjing, Jiangsu 211189, PR China

∗ Corresponding author. E-mail address: qizhengjian@seu.edu.cn (Z. Qi).

Supporting Information

General Information. All experimental materials and solvents were obtained from commercial approach without any further purification if not particularly mentioned. ^{1}H NMR and ^{13}C NMR spectra were performed on a Bruker Advance 600 MHz using DMSO-d6, $CDCl_3$ and acetone-d6 as solvents at room temperature. Molecular masses were measured on matrix-assisted laser desorptionionization time-of-flight mass spectrometry (MALDI-TOF-MS) using a BRUKER DALTONICS instrument and a-cyanohydroxycinnamic acid was selected as a matrix. UV-Vis absorption spectra were measured on UV-2600 (Shimadzu Corporation) and photoluminescence emission spectra were obtained from Fluoromax-4 (Horiba Jobin Yvon Inc) spectrophotometer. The solid and solution PL quantum efficiencies of the targeted product were measured using an integrating sphere under nitrogen at room temperature. Thermo gravimetric analysis (TGA) was performed with Netzsch simultaneous thermal analyzer (STA) system (STA409 PC) under a dry nitrogen gas flow at a heating rate of 10 ℃ min^{-1}. Differential scanning calorimetry (DSC) curves were measured using a Netzsch instrument (TA, Netzsch). The particle size distribution was measured by dynamic light scattering (DLS) using a BROOKHAVEN instrument. The film surface morphology was determined by atomic force microscopy (AFM) (Seiko Instruments, SPA-400). X-ray diffraction (XRD) analyses were measured on a BRUKER D8-DISCOVER diffractometer using Cu Kα radiation. Cyclic voltammogram was performed in CH_2Cl_2 solution (10^{-3} M) with tetrabutylammonium hexafluorophosphate (0.1 M) as supporting electrolyte and ferrocene as the internal standard at a scant rate of 100 mV s^{-1} on CHI750C voltammetric analyzer. A platinum plate, silver wire and aplatinum wire were used as the working, reference and counter electrode, respectively.

Device Fabrication and Measurements. Prior to use, the glass substrates were coated with indium tin oxide (ITO) with a sheet resistance of 15 Ω per square and then sequentially cleaned in an ultrasonic bath with deionized water, acetone and ethanol for 15 minutes. The ITO layer was produced by magnetron sputtering

technology with a roughness of 9.8 Å. A PEDOT:PSS layer (50 nm) was spin-coated onto the ITO surface and baked at 150 ℃ for 10 min to remove the residual water. Then, an EML with a thickness of about 40 nm was spin-coated from a filtered 10 mg mL^{-1} 1, 2-dichloroethane solution onto the PEDOT: PSS layer and annealed at 80 ℃ for 30 min to remove the residual solvent under N_2 atmosphere. Then, an electron-transport layer TPBi, a Cs_2CO_3 layer and an Al layer were deposited consecutively onto the spin-coated film in a vacuum chamber at ~ 4×10^{-4} Pa with the deposition rates of 1-2 Å s^{-1}, 0.1 Å s^{-1}, 6 Å s^{-1}, respectively. The emission area was 2×2 mm^{-2} controlled through a shadow mask. All the characterizations were measured immediately after manufacture at room temperature in ambient condition without encapsulation. The current density and luminance versus driving voltage curves and electroluminescence spectra were measured by a Keithley 2400s source meter and PR655 spectra colorimeter. External quantum efficiencies of the devices were calculated assuming a Lambertian emission distribution.

Calculation of rate constants[1-2]

$$k_{r,\,S} = \frac{\Phi_p}{\tau_p} \quad (1)$$

$$k_{nr,\,S} = k_{r,\,S}\left(\frac{1-\Phi_{PL}}{\Phi_{PL}}\right) \quad (2)$$

$$k_{ISC} = k_{r,\,S}\left(\frac{1}{\Phi_p}-\frac{1}{\Phi_{PL}}\right) \quad (3)$$

$$k_{RISC} = \frac{\Phi_{PL}}{k_{r,\,S}\,\tau_p\,\tau_d} \quad (4)$$

$$\Phi_{p=}\frac{A_1\tau_p}{A_1\tau_p + A_2\tau_d}\Phi_{PL} \quad (5)$$

$$\Phi_{d=}\frac{A_2\tau_d}{A_1\tau_p + A_2\tau_d}\Phi_{PL} \quad (6)$$

The rate constants were calculated according to above equation (1)-(6): Where τ_p and

τ_d were the lifetimes of the prompt and delayed decay components, respectively. Φ_{PL} and Φ_P were the total PL quantum yield, prompt fluorescence and delayed fluorescence quantum yield, respectively. $k_{r,\,S}$, $k_{nr,\,S}$, k_{ISC} and k_{RISC} were the rate constant for fluorescence radiative transition, non-radiative transition, intersystem crossing (ISC) and reverse intersystem crossing (RISC) processes, respectively. A_1 and A_2 were the frequency factors according to the followed fitting model of transient PL decay curves : $I(t) = A_1 \exp\left(-\frac{t}{\tau_p}\right) + A_2 \exp\left(-\frac{t}{\tau_d}\right)$.

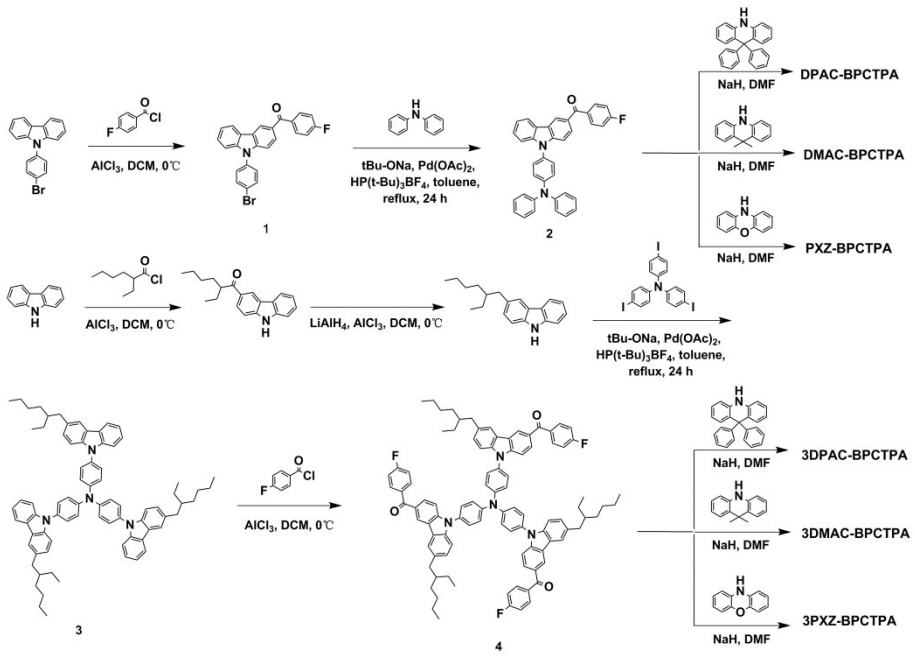

Scheme S1. The synthetic routes of these emitters.

Synthesis of (9-(4-bromophenyl)-9H-carbazol-3-yl)(4-fluorophenyl)methanone (1). To a solution of 9-(4-bromophenyl)-9H-carbazole (5 g, 15.5 mmol) and aluminium chloride (2.07 g, 15.5 mmol) in 50 mL dry dichloromethane at 0 ℃, 4-fluorobenzoyl chloride (2.95 mg, 18.6 mmol) was added dropwise. After the addition was completed, the mixture was stirred at room temperature for 12 h. The reaction was quenched by adding 40 mL ice-HCl solution, and the aqueous layer was

separated from the organic layer. Then the aquatic phase was further extracted with dichloromethane for several times. The combined organic solution was evaporated under vacuo to afford intermediate products. The solvent was removed under reduced pressure and the residue was purified on a silica gel column using petroleum ether/dichloromethane mixture (4:1, v/v) as eluent to afford the product as white powder in 91% yield. ^{1}H NMR (600 MHz, DMSO-d6) δ [ppm]: 8.71 (d, J = 1.4 Hz, 1H), 8.39 (d, J = 7.7 Hz, 1H), 7.92-7.85 (m, 5H), 7.67-7.65 (m, 2H), 7.51 (ddd, J = 13.7, 7.7, 3.8 Hz, 2H), 7.45-7.41 (m, 3H), 7.38-7.35 (m, 1H). ^{13}C NMR (150 MHz, DMSO-d6) δ [ppm]: 194.51, 165.69, 164.03, 142.92, 141.36, 135.97, 135.20, 135.19, 133.79, 132.92, 132.86, 129.76, 129.58, 128.95, 127.72, 123.89, 123.30, 123.10, 121.75, 121.65, 121.52, 116.12, 115.97, 110.55, 110.07. MS (MALDI-TOF) [m/z]: calcd for $C_{25}H_{15}BrFNO$, 443.03; found, 443.040.

Synthesis of (9-(4-(diphenylamino)phenyl)-9H-carbazol-3-yl)(4-fluorophenyl)methanone (2). 2 (4 g, 9 mmol), diphenylamine (1.98 g, 11.7 mmol), $Pd(OAc)_2$ (51.6 mg, 0.23 mmol), $HP(t\text{-}Bu)_3BF_4$ (66.7 mg, 0.23 mmol), t-BuONa (1.69 g, 17.55 mmol) were dissolved in 30 mL toluene and refluxed for 24 h under nitrogen. After cooled, the mixture was extracted with dichloromethane and washed with brine for three times. After dried over anhydrous Na_2SO_4, the solvent was removed under reduced pressure and the residue was purified with column chromatography on silica gel using petroleum ether/dichloromethane mixture (3:1, v/v) as the eluent to afford the product as white powder in 87% yield. ^{1}H NMR (600 MHz, DMSO-d6) δ [ppm]: 8.69 (d, J = 1.4 Hz, 1H), 8.37 (d, J = 7.8 Hz, 1H), 7.91-7.86 (m, 3H), 7.56-7.49 (m, 4H), 7.41 (ddd, J = 15.9, 8.3, 4.2 Hz, 7H), 7.34 (dd, J = 11.3, 4.3 Hz, 1H), 7.23-7.17 (m, 6H), 7.14 (t, J = 7.4 Hz, 2H). ^{13}C NMR (150 MHz, DMSO-d6) δ [ppm]: 194.49, 147.62, 147.30, 143.31, 141.79, 135.29, 135.27, 132.90, 132.8, 130.26, 130.02, 129.36, 128.77, 128.39, 127.53, 125.21, 124.30, 123.92, 123.59, 123.07, 122.78, 121.61, 121.30, 116.07, 115.93, 110.69, 110.13. MS (MALDI-TOF)

[m/z]: calcd for $C_{37}H_{25}FN_2O$, 532.20; found, 532.246.

Synthesis of tris(4-(3-(2-ethylhexyl)-9H-carbazol-9-yl)phenyl)amine (3). tris(4-iodophenyl)amine (4 g, 6.13 mmol), 3-(2-ethylhexyl)-9H-carbazole (6.85 g, 24.52 mmol), $Pd(OAc)_2$ (110 mg, 0.49 mmol), $HP(t\text{-}Bu)_3BF_4$ (142.2 mg, 0.49 mmol), t-BuONa (3.53 g, 36.78 mmol) were dissolved in 60 mL toluene and refluxed for 24 h under nitrogen. After cooled, the mixture was extracted with dichloromethane and washed with brine for three times. After dried over anhydrous Na_2SO_4, the solvent was removed under reduced pressure and the residue was purified with column chromatography on silica gel using petroleum ether/dichloromethane mixture (3:1, v/v) as the eluent to afford the product as white powder in 83% yield. ^{1}H NMR (600 MHz, DMSO-d6) δ [ppm]: 8.23 (d, J = 7.6 Hz, 3H), 8.02 (s, 3H), 7.67 (d, J = 8.4 Hz, 6H), 7.55 (d, J = 8.5 Hz, 6H), 7.50-7.36 (m, 9H), 7.33-7.23 (m, 6H), 2.70 (d, J = 6.8 Hz, 6H), 1.69-1.64 (m, 3H), 1.45-1.20 (m, 24H), 0.87 (dt, J = 18.5, 7.0 Hz, 18H). ^{13}C NMR (150 MHz, $CDCl_3$) δ [ppm]:141.11, 139.41, 133.54, 133.07, 128.07, 127.44, 125.71, 125.33, 123.34, 123.31, 120.47, 120.26, 119.72, 109.77, 109.35, 41.71, 40.15, 32.36, 28.93, 25.42, 23.11, 14.19, 10.87. MS (MALDI-TOF) [m/z]: calcd for $C_{78}H_{84}N_4$, 1076.67; found, 1076.679.

Synthesis of ((nitrilotris(benzene-4,1-diyl))tris(6-(2-ethylhexyl)-9H-carbazole-9,3-diyl))tris((4-fluorophenyl)methanone) (4). The synthetic process of 4 was similar to that for 1 as green powder with a yield of 90%. ^{1}H NMR (600 MHz, DMSO-d6) δ [ppm]: 8.68 (d, J = 1.5 Hz, 3H), 8.18 (s, 3H), 7.89 (ddd, J = 12.9, 7.2, 1.8 Hz, 9H), 7.72 (d, J = 8.7 Hz, 6H), 7.58 (t, J = 8.5 Hz, 9H), 7.48-7.37 (m, 9H), 7.33 (dd, J = 9.8, 1.4 Hz, 3H), 2.69 (d, J = 6.9 Hz, 6H), 1.67 (dt, J = 12.2, 6.1 Hz, 3H), 1.35-1.19 (m, 24H), 0.85 (dt, J = 15.4, 7.2 Hz, 18H). ^{13}C NMR (150 MHz, $CDCl_3$) δ [ppm]: 195.17, 165.88, 164.21, 146.64, 143.56, 140.20, 135.07, 135.05, 134.86, 132.52, 132.46, 132.39, 129.29, 128.34, 128.23, 125.48, 115.43, 115.29, 109.82, 41.68, 40.12, 32.30,

28.88, 25.36, 23.10, 14.18, 10.84. MS (MALDI-TOF) [m/z]: calcd for $C_{99}H_{93}F_3N_4O_3$, 1443.72; found, 1443.724.

Synthesis of (4-(9,9-diphenylacridin-10(9H)-yl)phenyl)(9-(4-(diphenylamino)phenyl)-9H-carbazol-3-yl)methanone (DPAC-BPCTPA). 9,9-diphenyl-9,10-dihydroacridine (406.78 mg, 1.22 mmol) was dissolved in 15 mL dry dimethylformamide (DMF) and t-BuOK (210.95 mg, 1.88 mmol) was added under nitrogen atmosphere. The mixture was stirred at room temperature for 30 minutes. Then, 2 (500 mg, 0.94 mmol) was dissolved in 5 mL dry dimethylformamide (DMF) and added to the mixture dropwise. After the addition was completed, the mixture was stirred at 110 ℃ for 12 h. After cooling to room temperature, the resulting mixture was poured into water and extracted with ethyl acetate for three times. The combined organic solution were washed with brine three times. After dried over anhydrous $MgSO_4$, the solvent was removed under reduced pressure and the residue was purified with column chromatography on silica gel using petroleum ether/dichloromethane mixture (2:1, v/v) as the eluent to afford the product as green powder in 87% yield. ^{1}H NMR (600 MHz, DMSO-d6) δ [ppm]: 8.81 (d, J = 1.5 Hz, 1H), 8.41 (d, J = 7.8 Hz, 1H), 8.02 (d, J = 8.3 Hz, 2H), 7.98 (dd, J = 8.6, 1.7 Hz, 1H), 7.57-7.50 (m, 4H), 7.44 (d, J = 8.2 Hz, 1H), 7.41-7.38 (m, 4H), 7.37-7.31 (m, 5H), 7.28 (t, J = 7.6 Hz, 4H), 7.22-7.18 (m, 6H), 7.17-7.12 (m, 4H), 6.95 (ddd, J = 11.8, 8.3, 4.1 Hz, 6H), 6.81 (dd, J = 7.8, 1.4 Hz, 2H), 6.51 (dd, J = 8.2, 0.7 Hz, 2H). ^{13}C NMR (150 MHz, DMSO-d6) δ [ppm]: 195.02, 147.64, 147.31, 146.43, 141.82, 141.70, 132.63, 131.13, 130.27, 130.09, 130.02, 129.70, 128.42, 128.33, 127.74, 127.57, 127.02, 125.22, 124.31, 123.60, 121.12, 114.70. MS (MALDI-TOF) [m/z]: calcd for $C_{62}H_{43}N_3O$, 845.34; found, 846.332. Melting point: 174.3°. Anal. Calcd for $C_{62}H_{43}N_3O$: C, 88.02; H, 5.12; N, 4.97; O, 1.89. Found: C, 88.10; H, 5.04; N, 5.06.

Synthesis of (4-(9,9-dimethylacridin-10(9H)-yl)phenyl)(9-(4-

(diphenylamino)phenyl)-9H-carbazol-3-yl)methanone (DMAC-BPCTPA).

The synthetic process of DMAC-BPCTPA was similar to that for DPAC-BPCTPA as green powder with a yield of 88%. ^{1}H NMR (600 MHz, DMSO-d6) δ [ppm]: 8.85 (d, J = 1.6 Hz, 1H), 8.42 (d, J = 7.8 Hz, 1H), 8.09 (d, J = 8.3 Hz, 2H), 8.01 (dd, J = 8.6, 1.6 Hz, 1H), 7.62-7.50 (m, 9H), 7.45 (d, J = 8.2 Hz, 1H), 7.42-7.36 (m, 5H), 7.20 (dd, J = 10.7, 8.2 Hz, 6H), 7.14 (t, J = 7.4 Hz, 2H), 7.07-7.03 (m, 2H), 6.34 (dd, J = 8.2, 0.8 Hz, 2H), 1.65 (s, 6H). ^{13}C NMR (150 MHz, DMSO-d6) δ [ppm]: 195.10, 147.64, 147.32, 140.53, 132.88, 131.25, 130.60, 130.28, 130.04, 128.43, 127.05, 125.92, 125.22, 124.31, 123.62, 121.73, 121.42, 121.33, 114.56, 36.14, 31.56. MS (MALDI-TOF) [m/z]: calcd for $C_{52}H_{39}N_3O$, 721.31; found, 722.300. Melting point: 155.6°. Anal. Calcd for $C_{52}H_{39}N_3O$: C, 86.52; H, 5.45; N, 5.82; O, 2.22. Found: C, 86.50; H, 5.51; N, 5.87.

Synthesis of (4-(10H-phenoxazin-10-yl)phenyl)(9-(4-(diphenylamino)phenyl)-9H-carbazol-3-yl)methanone (PXZ-BPCTPA).

The synthetic process of PXZ-BPCTPA was similar to that for DPAC-BPCTPA as yellow powder with a yield of 82%. ^{1}H NMR (600 MHz, $CDCl_3$) δ [ppm]: 8.73 (d, J = 1.5 Hz, 1H), 8.20 (d, J = 7.8 Hz, 1H), 8.09 (d, J = 8.2 Hz, 2H), 8.01 (dd, J = 8.6, 1.7 Hz, 1H), 7.53-7.47 (m, 5H), 7.41-7.38 (m, 2H), 7.36-7.31 (m, 5H), 7.29-7.27 (m, 2H), 7.24-7.21 (m, 4H), 7.11 (t, J = 7.3 Hz, 2H), 6.73 (dd, J = 7.7, 1.5 Hz, 2H), 6.71-6.63 (m, 4H), 6.05 (d, J = 7.8 Hz, 2H). ^{13}C NMR (150 MHz, $CDCl_3$) δ [ppm]: 195.49, 147.82, 147.33, 144.01, 143.82, 142.27, 142.04, 138.85, 133.88, 132.68, 130.73, 130.08, 129.55, 128.89, 128.66, 127.81, 126.82, 125.01, 123.78, 123.71, 123.56, 123.30, 123.22, 123.02, 121.76, 120.87, 120.70, 115.64, 113.39, 110.45, 109.63. MS (MALDI-TOF) [m/z]: calcd for $C_{49}H_{33}N_3O_2$, 695.26; found, 696.250. Melting point: 183.4°. Anal. Calcd for $C_{49}H_{33}N_3O_2$: C, 84.58; H, 4.78; N, 6.04; O, 4.60. Found: C, 84.51; H, 4.82; N, 6.11.

Synthesis of ((nitrilotris(benzene-4,1-diyl))tris(6-((S)-2-ethylhexyl)-9H-carbazole-9,3-diyl))tris((4-(9,9-diphenylacridin-10(9H)-yl)phenyl)methanone) (3DPAC-BPCTPA).

9,9-diphenyl-9,10-dihydroacridine (733.55 mg, 2.2 mmol) was dissolved in 15 mL dry dimethylformamide (DMF) and t-BuOK (123.3 mg, 1.1 mmol) was added under nitrogen atmosphere. The mixture was stirred at room temperature for 30 minutes. Then, 4 (800 mg, 0.55 mmol) was dissolved in 10 mL dry dimethylformamide (DMF) and added to the mixture dropwise. After the addition was completed, the mixture was stirred at 110 ℃ for 12 h. After cooling to room temperature, the resulting mixture was poured into water and extracted with ethyl acetate for three times. The combined organic solution was washed with brine three times. After dried over anhydrous $MgSO_4$, the solvent was removed under reduced pressure and the residue was purified with column chromatography on silica gel using petroleum ether/dichloromethane mixture (2:1, v/v) as the eluent to afford the product as green powder in 74% yield.

^{1}H NMR (600 MHz, Acetone-d6) δ [ppm]: 8.69 (d, J = 1.5 Hz, 3H), 8.04 (s, 3H), 7.96 (d, J = 8.3 Hz, 6H), 7.91 (dd, J = 8.6, 1.6 Hz, 3H), 7.64 (d, J = 8.8 Hz, 6H), 7.59 (d, J = 8.8 Hz, 6H), 7.49 (d, J = 8.6 Hz, 3H), 7.35 (d, J = 8.4 Hz, 3H), 7.27 (dd, J = 8.4, 1.4 Hz, 3H), 7.23-7.12 (m, 24H), 7.04-7.00 (m, 6H), 6.89-6.85 (m, 9H), 6.84-6.81 (m, 6H), 6.76 (dd, J = 7.8, 1.5 Hz, 6H), 6.46 (dd, J = 8.2, 0.9 Hz, 6H), 2.66-2.66 (m, 6H), 1.60 (s, 3H), 1.16 (t, J = 9.2 Hz, 25H), 0.74 (td, J = 7.1, 4.0 Hz, 18H). ^{13}C NMR (150 MHz, $CDCl_3$) δ [ppm]: 195.61, 146.68, 146.27, 144.22, 143.71, 141.88, 140.26, 138.47, 134.94, 132.41, 132.19, 131.02, 130.39, 130.17, 130.12, 129.12, 128.57, 128.38, 128.27, 127.67, 126.92, 126.36, 125.50, 123.82, 123.41, 123.15, 120.94, 120.59, 114.24, 109.84, 109.45, 56.82, 41.68, 40.16, 32.33, 28.89, 25.40, 23.10, 14.18, 10.86. MS (MALDI-TOF) [m/z]: calcd for $C_{174}H_{147}N_7O_3$, 2383.16; found, 2384.073. Melting point: 191.4°. Anal. Calcd for $C_{174}H_{147}N_7O_3$: C, 87.66; H, 6.22; N, 4.11; O, 2.01. Found: C, 87.59; H, 6.27; N, 4.06.

Synthesis of ((nitrilotris(benzene-4,1-diyl))tris(6-((S)-2-ethylhexyl)-9H-carbazole-9,3-diyl))tris((4-(9,9-dimethylacridin-10(9H)-yl)phenyl)methanone) (3DMAC-BPCTPA).

The synthetic process of 3DMAC-BPCTPA was similar to that for 3DPAC-BPCTPA as green powder with a yield of 77%. ^{1}H NMR (600 MHz, $CDCl_3$) δ [ppm]: 8.78 (d, J = 1.3 Hz, 3H), 8.14 (d, J = 8.2 Hz, 6H), 8.06 (dd, J = 8.7, 1.5 Hz, 3H), 8.00 (s, 3H), 7.63 (d, J = 8.7 Hz, 6H), 7.58 (dd, J = 8.6, 1.8 Hz, 9H), 7.52 (d, J = 8.2 Hz, 6H), 7.51-7.47 (m, 6H), 7.45 (d, J = 8.3 Hz, 3H), 7.32 (dd, J = 8.4, 1.0 Hz, 3H), 7.06-7.01 (m, 6H), 6.97 (t, J = 7.4 Hz, 6H), 6.40 (d, J = 8.1 Hz, 6H), 2.80-2.72 (m, 6H), 1.74-1.66 (m, 21H), 1.37-1.28 (m, 24H), 0.93-0.87 (m, 19H). ^{13}C NMR (150 MHz, $CDCl_3$) δ [ppm]: 195.64, 146.70, 144.73, 143.75, 140.58, 138.46, 134.95, 132.58, 132.42, 131.03, 130.49, 129.15, 128.64, 128.41, 128.29, 126.42, 125.51, 125.36, 123.82, 123.43, 123.22, 121.02, 114.27, 109.86, 109.45, 41.69, 40.17, 36.07, 32.34, 31.14, 28.90, 25.40, 23.10, 14.18, 10.86. MS (MALDI-TOF) [m/z]: calcd for $C_{144}H_{135}N_7O_3$, 2011.07; found, 2011.983. Melting point: 164.6°. Anal. Calcd for $C_{144}H_{135}N_7O_3$: C, 85.98; H, 6.76; N, 4.87; O, 2.39. Found: C, 85.91; H, 6.81; N, 4.80.

Synthesis of ((nitrilotris(benzene-4,1-diyl))tris(6-((S)-2-ethylhexyl)-9H-carbazole-9,3-diyl))tris((4-(10H-phenoxazin-10-yl)phenyl)methanone) (3PXZ-BPCTPA)

The synthetic process of 3PXZ-BPCTPA was similar to that for 3DPAC-BPCTPA as yellow powder with a yield of 71%. ^{1}H NMR (600 MHz, $CDCl_3$) δ [ppm]: 8.75 (d, J = 1.1 Hz, 3H), 8.11 (d, J = 7.9 Hz, 6H), 8.04-7.97 (m, 6H), 7.63 (d, J = 8.7 Hz, 6H), 7.60-7.54 (m, 9H), 7.52 (d, J = 8.1 Hz, 6H), 7.45 (d, J = 8.3 Hz, 3H), 7.32 (dd, J = 8.4, 1.2 Hz, 3H), 6.76-6.58 (m, 18H), 6.05 (d, J = 6.6 Hz, 6H), 2.80-2.71 (m, 6H), 1.68 (dd, J = 11.8, 5.8 Hz, 3H), 1.37-1.27 (m, 24H), 0.90 (dt, J = 18.8, 7.2 Hz, 18H). ^{13}C NMR (150 MHz, $CDCl_3$) δ [ppm]: 195.44, 146.69, 144.08, 143.75, 140.26, 138.79, 134.97, 133.73, 132.70, 132.37, 130.85, 128.99, 128.99, 128.61, 128.43, 128.27, 125.50, 123.78, 123.39, 123.39, 123.24, 123.22, 121.90, 120.93, 115.65, 113.39, 109.86,

109.44, 99.97, 41.68, 40.14, 32.31, 28.89, 25.38, 23.10, 14.19, 10.82. MS (MALDI-TOF) [m/z]: calcd for $C_{135}H_{117}N_7O_6$, 1932.91; found, 1932.882. Melting point: 187.5°. Anal. Calcd for $C_{135}H_{117}N_7O_6$: C, 83.86; H, 6.10; N, 5.07; O, 4.96. Found: C, 83.79; H, 6.19; N, 4.55.

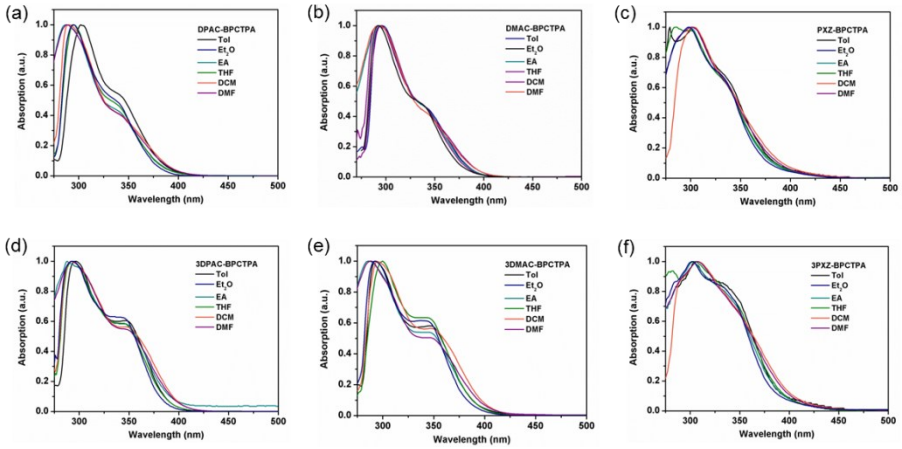

Figure S1. The UV-vis absorption spectra of DPAC-BPCTPA (a), DMAC-BPCTPA (b), 3PXZ-BPCTPA (c), 3DPAC-BPCTPA (d), 3DMAC-BPCTPA (e) and 3PXZ-BPCTPA (f) in various solvents at room temperature.

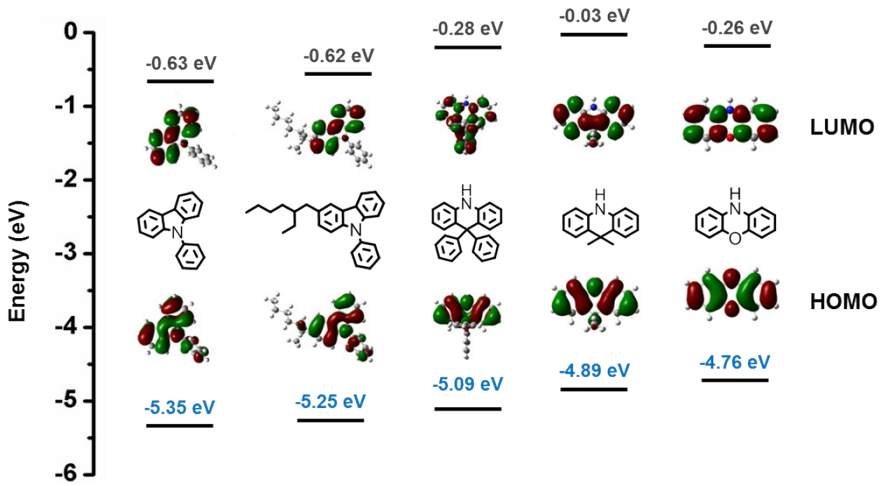

Figure S2. The molecular simulation results of 9-phenyl-9H-carbazole, 3-(2-ethylhexyl)-9-phenyl-9H-carbazole, DPAC, DMAC and PXZ units using the B3LYP functional and 6-31G (d) basis set.

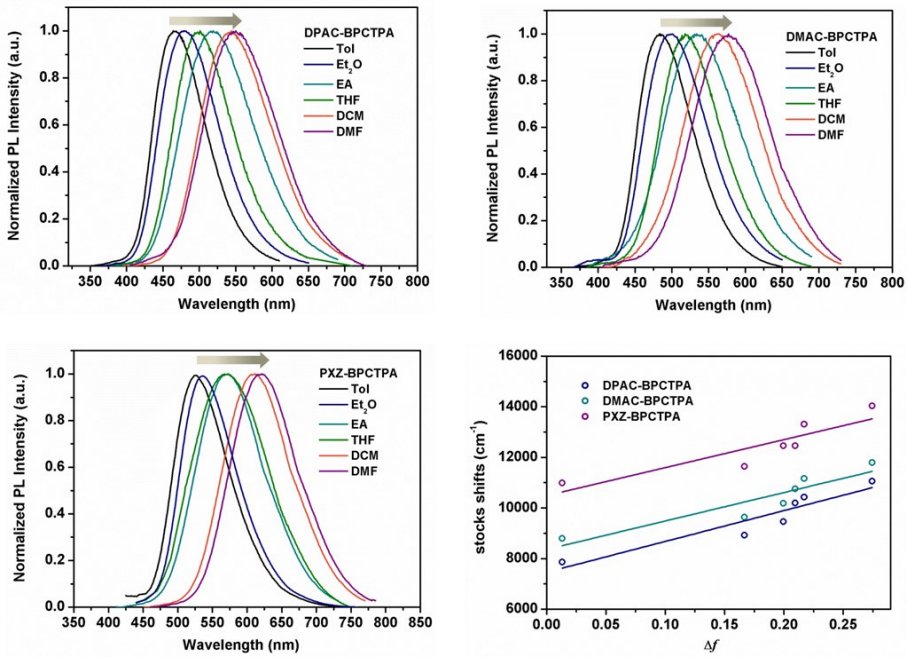

Figure S3. PL spectra of DPAC-BPCTPA (a), DMAC-BPCTPA (b) and 3PXZ-BPCTPA (c) in various solvents at room temperature. (d) Plot of Stokes shift versus orientation polarization (Δf) of the solvents.

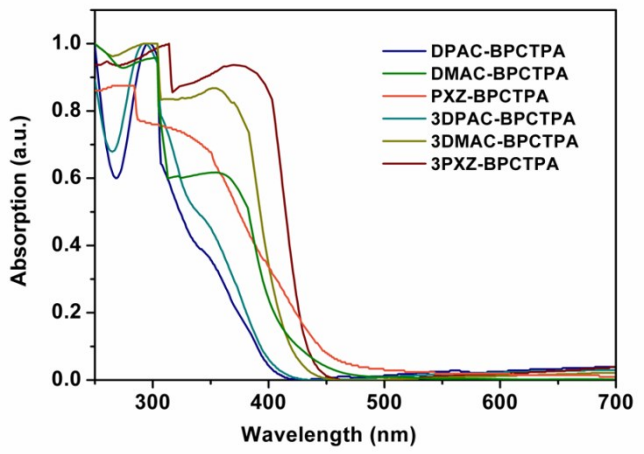

Figure S4. The UV-vis absorption spectra measured in neat films at room temperature.

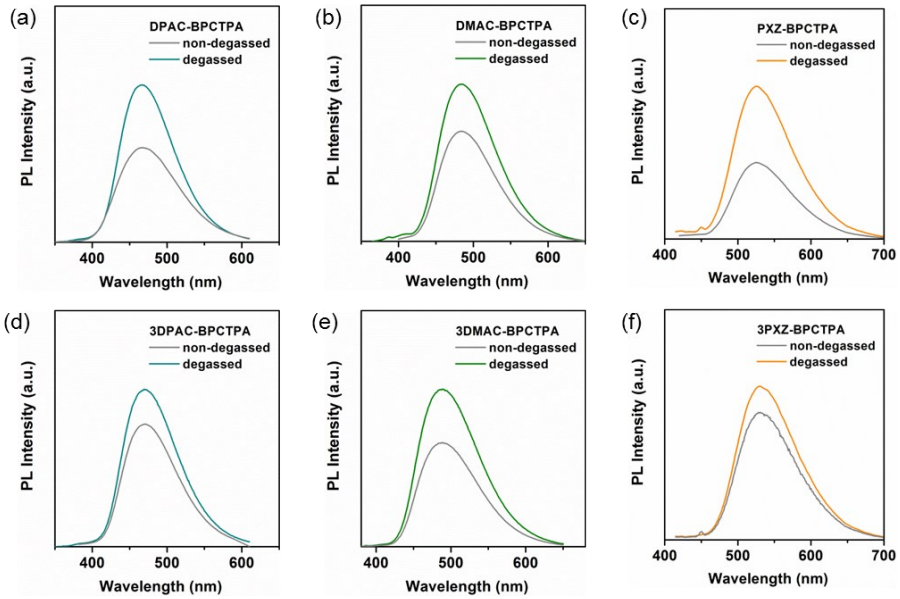

Figure S5. The PL spectra of of DPAC-BPCTPA (a), DMAC-BPCTPA (b), PXZ-BPCTPA (c), 3DPAC-BPCTPA (d), 3DMAC-BPCTPA (e) and 3PXZ-BPCTPA (f) in non-degassed and degassed toluene solution (10^{-5} M).

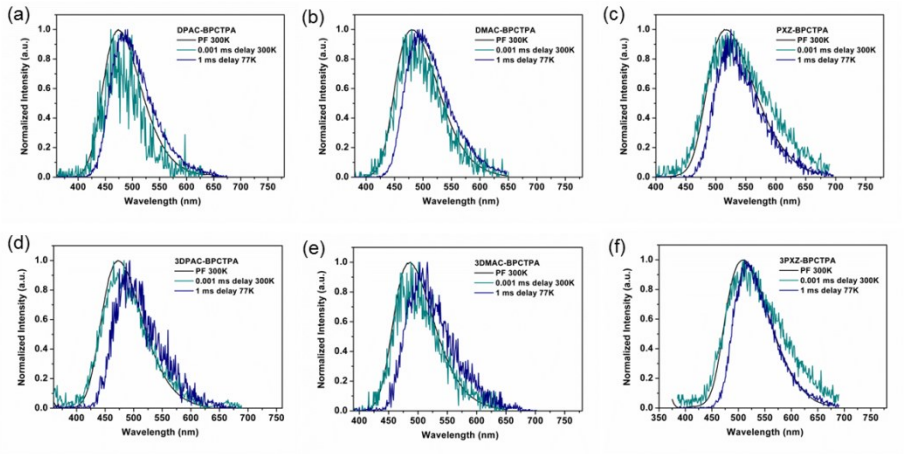

Figure S6. PF, DF and PH spectra of DPAC-BPCTPA (a), DMAC-BPCTPA (b), PXZ-BPCTPA (c), 3DPAC-BPCTPA (d), 3DMAC-BPCTPA (e) and 3PXZ-BPCTPA (f) in 20 wt% mCP films performed at 300 K and 77 K.

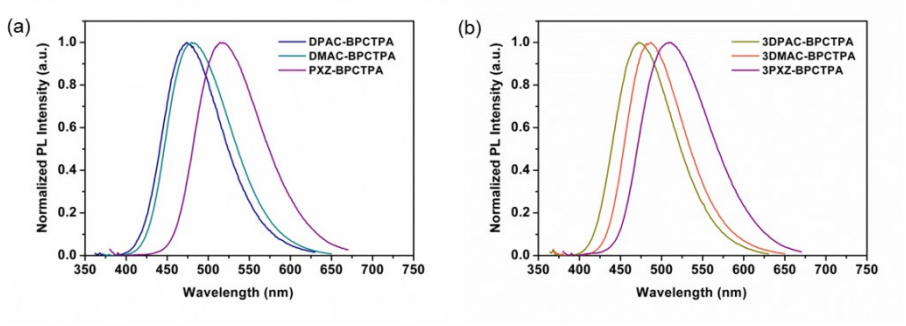

Figure S7. (a) The PL spectra of DPAC-BPCTPA, DMAC-BPCTPA and PXZ-BPCTPA in 20 wt% mCP films at room temperature. (b) The PL spectra of 3DPAC-BPCTPA, 3DMAC-BPCTPA and 3PXZ-BPCTPA in 20 wt% mCP films at room temperature.

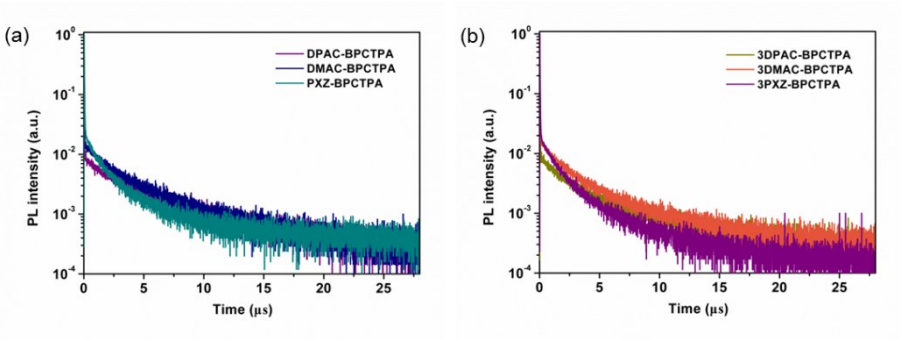

Figure S8. (a) The room-temperature fluorescence decay curves of DPAC-BPCTPA, DMAC-BPCTPA and PXZ-BPCTPA in 20 wt% mCP films under N_2 atmosphere. (b) The room-temperature fluorescence decay curves of 3DPAC-BPCTPA, 3DMAC-BPCTPA and 3PXZ-BPCTPA in 20 wt% mCP films under N_2 atmosphere.

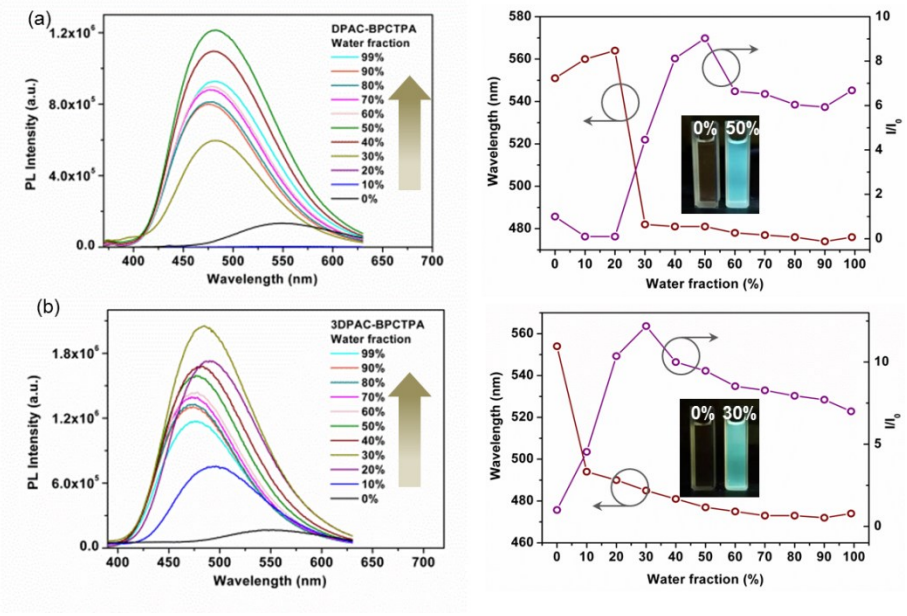

Figure S9. PL spectra of DPAC-BPCTPA (a) and 3DPAC-BPCTPA (c) in DMF/water mixtures at different water fractions. Plots of water fractions versus emission maximum wavelength and I/I_0 values of DPAC-BPCTPA (b) and 3DPAC-BPCTPA (d). I_0 is the PL intensity in pure DMF solution. Inset: photos of the emitters in corresponding DMF/water mixtures under 365 nm excitation.

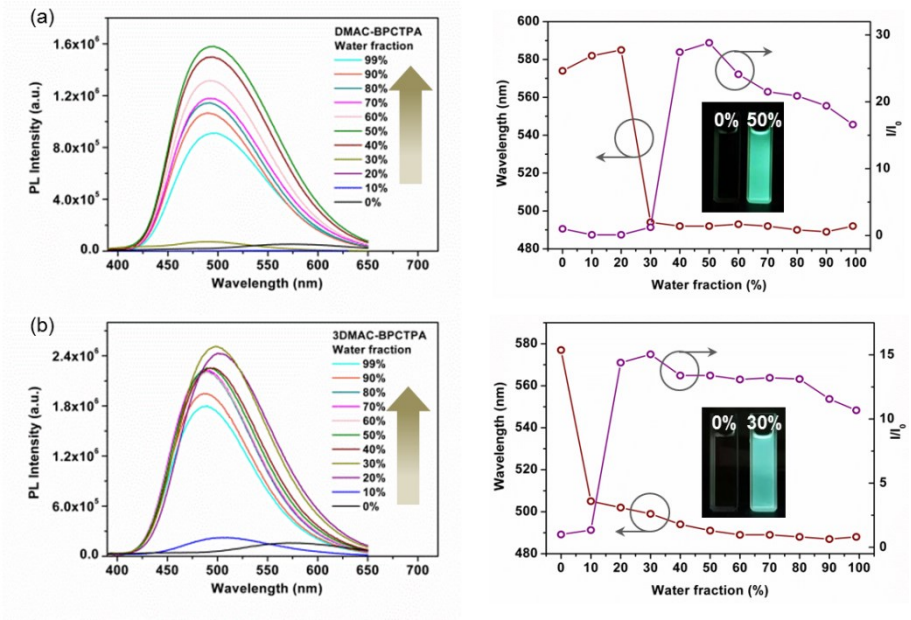

Figure S10. PL spectra of DMAC-BPCTPA (a) and 3DMAC-BPCTPA (c) in DMF/water mixtures at different water fractions. Plots of water fractions versus emission maximum wavelength and I/I_0 values of DMAC-BPCTPA (b) and 3DMAC-BPCTPA (d). I_0 is the PL intensity in pure DMF solution. Inset: photos of the emitters in corresponding DMF/water mixtures under 365 nm excitation.

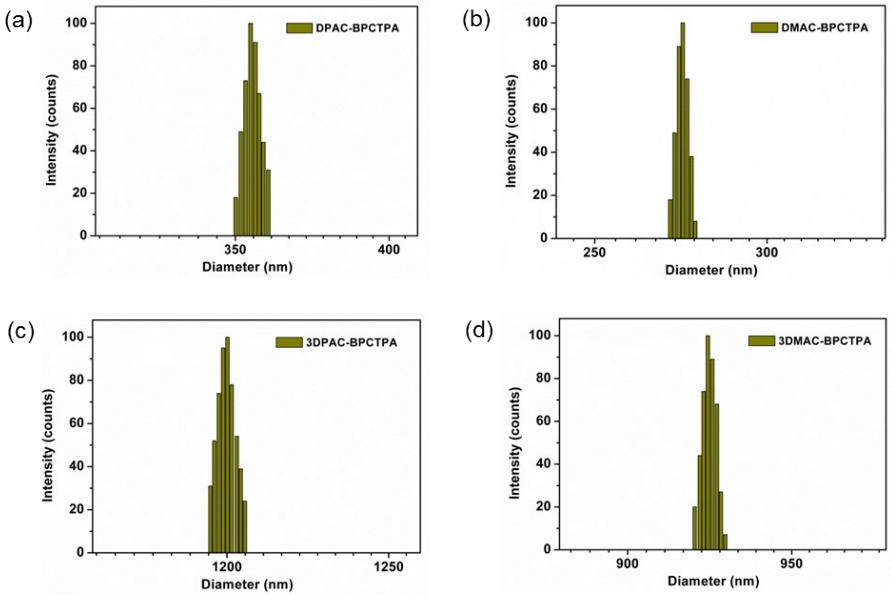

Figure S11. The particle size distributions of DPAC-BPCTPA (a), DMAC-BPCTPA

(a), 3DPAC-BPCTPA (c) and 3PXZ-BPCTPA (d) formed in the mixed solvent with 50% water fraction.

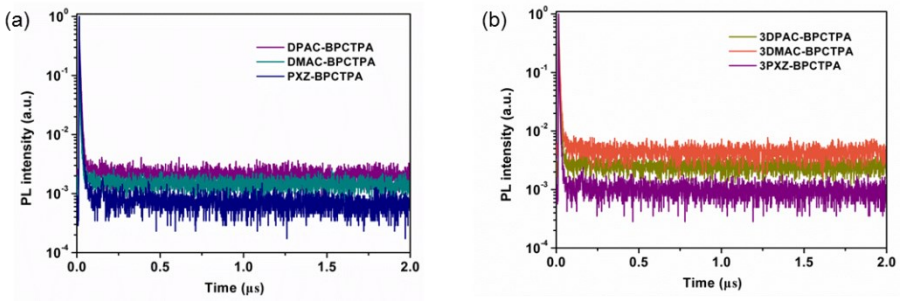

Figure S12. The transient PL decay spectra of DPAC-BPCTPA, DMAC-BPCTPA and PXZ-BPCTPA (a), 3DPAC-BPCTPA, 3DMAC-BPCTPA and 3PXZ-BPCTPA (b) in DMF solutions under N_2 atmosphere after N_2 bubbling at room temperature.

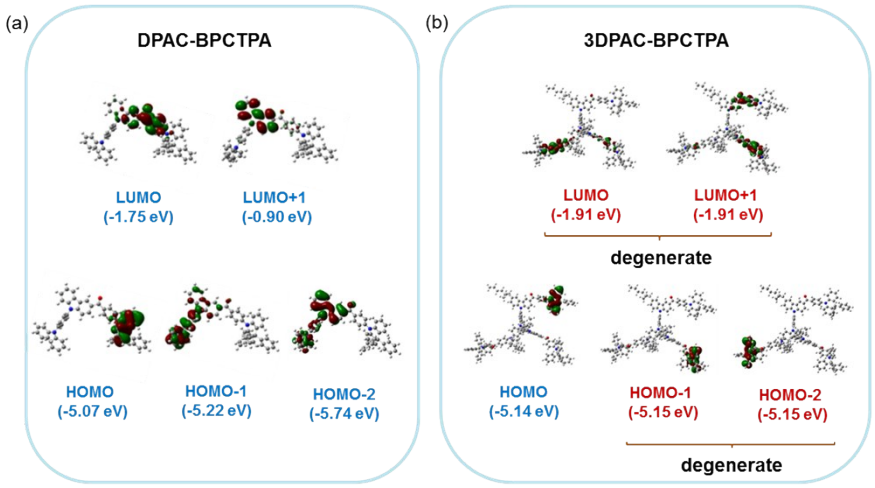

Figure S13. Frontier molecular orbitals distribution of DPAC-BPCTPA (a) and 3DPAC-BPCTPA (b).

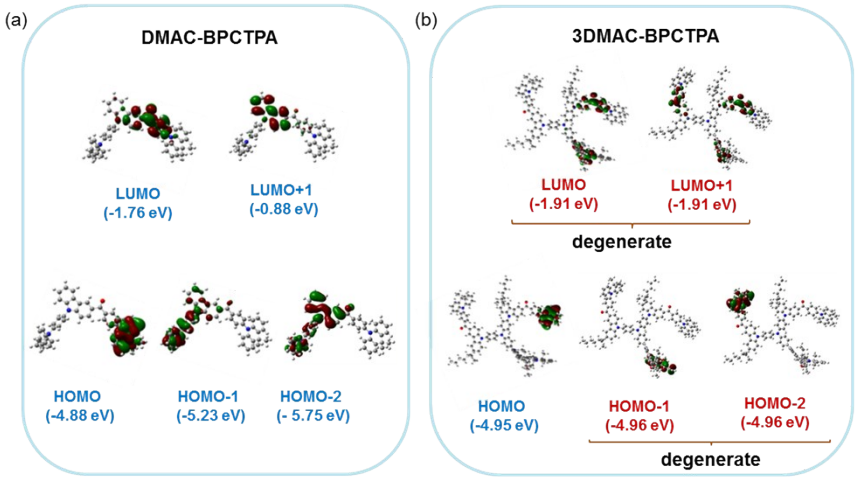

Figure S14. Frontier molecular orbitals distribution of DMAC-BPCTPA (a) and 3DMAC-BPCTPA (b).

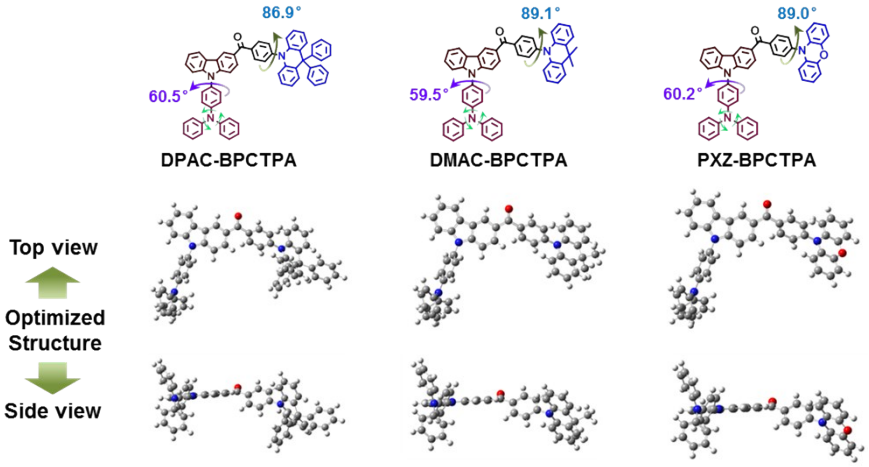

Figure S15. The optimized structures with twisted angles of DPAC-BPCTPA, DMAC-BPCTPA and PXZ-BPCTPA.

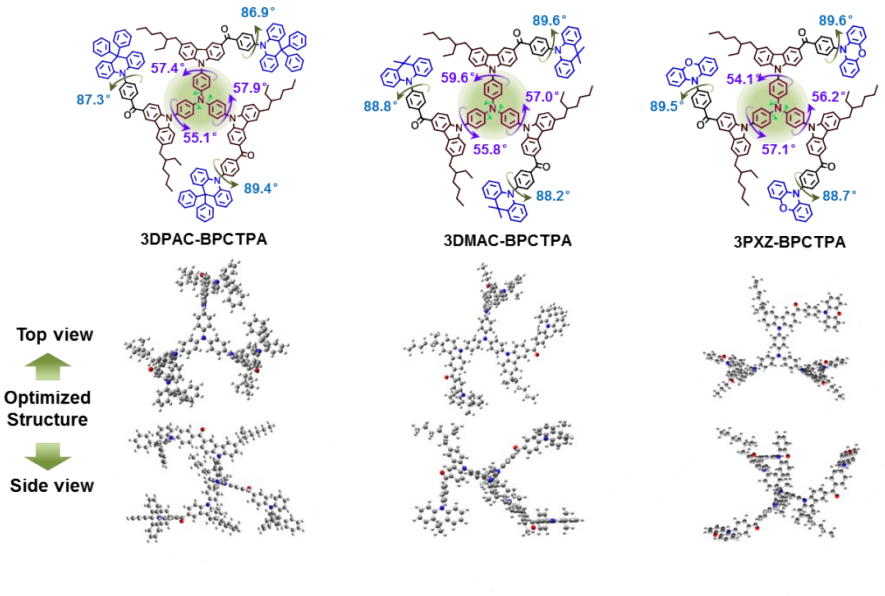

Figure S16. The optimized structures with twisted angles of 3DPAC-BPCTPA, 3DMAC-BPCTPA and 3PXZ-BPCTPA.

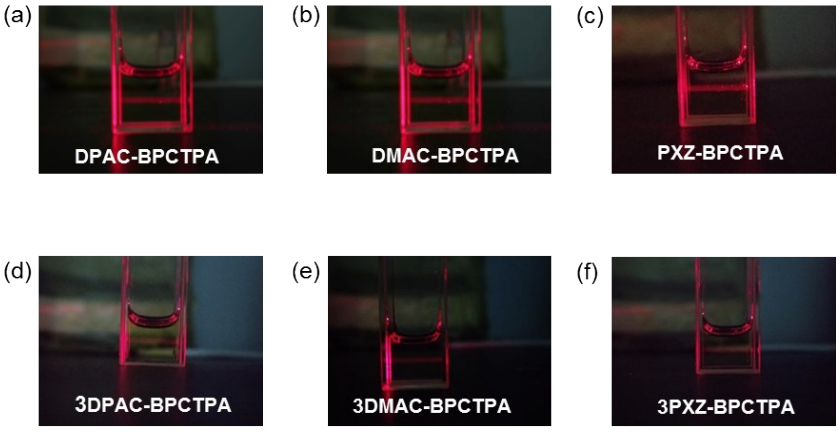

Figure S17. The photographs of Tyndall measurement in 1, 2-dichloroethane solution of DPAC-BPCTPA (a), DMAC-BPCTPA(b), PXZ-BPCTPA (c), 3DPAC-BPCTPA (d), 3DMAC-BPCTPA(e), 3PXZ-BPCTPA (f).

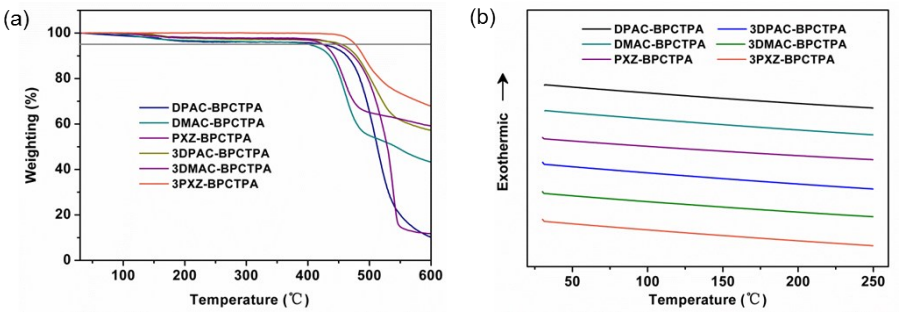

Figure S18. TGA(a) and DSC (b) curves of these emitters at a heating rate of 10℃ min^{-1} under nitrogen.

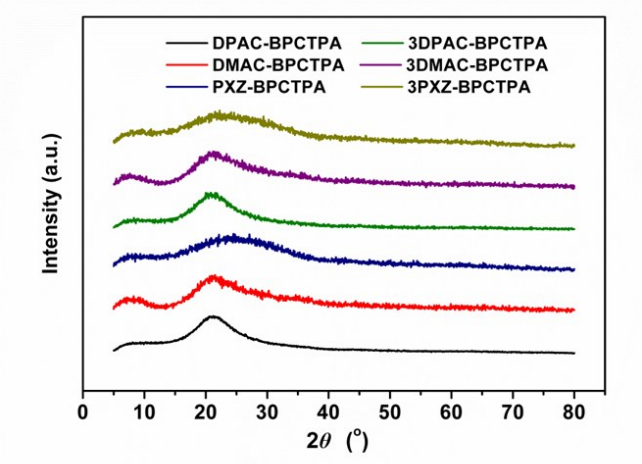

Figure S19. The XRD curves of these emitters in solution-processed neat films.

Table S1. Photophysical properties of these compounds in 20 wt% mCP films.

Compound	λ_{em}[a] [nm]	S_1[b] [eV]	T_1[c] [eV]	ΔE_{ST}[d] [eV]
DPAC-BPCTPA	474	2.99	2.84	0.15
DMAC-BPCTPA	481	2.92	2.79	0.13
PXZ-BPCTPA	517	2.71	2.62	0.09
3DPAC-BPCTPA	474	2.96	2.82	0.14
3DMAC-BPCTPA	488	2.86	2.75	0.11
3PXZ-BPCTPA	510	2.77	2.66	0.10

[c]Measured in neat film state. [d]Obtained from the onsets of absorption spectra in neat film. [g]Calculated from the onset of the fluorescence spectra in neat film at 300 K. [h]Obtained at 77 K in neat film. [i]Splitting between S_1 and T_1 energy.

Table S2. Photophysical properties of DPAC-BPCTPA, DMAC-BPCTPA and PXZ-BPCTPA in various solvents.

Solvent	DPAC-BPCTPA			DMAC-BPCTPA			PXZ-BPCTPA		
	λ_{abs} (nm)	λ_{em} (nm)	Stokes shift (cm^{-1})	λ_{abs} (nm)	λ_{em} (nm)	Stokes shift (cm^{-1})	λ_{abs} (nm)	λ_{em} (nm)	Stokes shift (cm^{-1})
Tol	340	465	7866	340	484	8793	333	525	10982
Et_2O	339	478	8621	341	499	9321	333	535	11338
EA	339	499	9458	339	518	10181	332	567	12455
THF	339	517	10193	339	534	10755	333	570	12455
DCM	342	543	10823	343	562	11361	333	609	13610
DMF	341	548	11058	343	577	11793	332	620	14030
Δμ (D)	17.9			18.8			19.6		

Table S3. Photophysical properties of 3DPAC-BPCTPA, 3DMAC-BPCTPA and 3PXZ-BPCTPA in various solvents.

Solvent	3DPAC-BPCTPA			3DMAC-BPCTPA			3PXZ-BPCTPA		
	λ_{abs} (nm)	λ_{em} (nm)	Stokes shift (cm^{-1})	λ_{abs} (nm)	λ_{em} (nm)	Stokes shift (cm^{-1})	λ_{abs} (nm)	λ_{em} (nm)	Stokes shift (cm^{-1})
Tol	343	470	7843	341	488	8809	336	531	10950
Et_2O	337	481	8889	337	500	9672	332	541	11681
EA	345	512	9455	339	519	10192	333	570	12492
THF	340	520	10188	340	537	10796	335	573	12421
DCM	345	539	10427	346	564	11186	334	602	13303
DMF	342	550	11056	342	575	11814	329	613	14040
Δμ (D)	21.1			22.7			23.9		

Table S4. The calculated electronic transitions by TD-DFT of DPAC-BPCTPA, DMAC-BPCTPA and PXZ-BPCTPA.

	Excited state 1	Excited state 2	Excited state 3
DPAC-BPCTPA	λ=463 nm f=0.000 HOMO->LUMO 98%	λ=389 nm f=0.1178 HOMO-1->LUMO 97%	λ=358 nm f=0.0004 HOMO-5->LUMO 68%
DMAC-BPCTPA	λ=480 nm f=0.000 HOMO->LUMO 98%	λ=395 nm f=0.1336 HOMO-1->LUMO 97%	λ=361 nm f=0.0008 HOMO-4->LUMO 68%
PXZ-BPCTPA	λ=529 nm f=0.000 HOMO->LUMO 98%	λ=401 nm f=0.1200 HOMO-1->LUMO 97%	λ=363 nm f=0.0039 HOMO-5->LUMO 68%

Table S5. Photophysical characteristics and kinetic parameters of these compounds in 20 wt% mCP films.

Compound	ϕ_{PL}[a] [%]	ϕ_p[b] [%]	ϕ_d[b] [%]	τ_p[b] [ns]	τ_d[b] [μs]	$k_{r,S}$[c] [10^6 s^{-1}]	$k_{nr,S}$[c] [10^6 s^{-1}]	k_{ISC}[c] [10^7 s^{-1}]	k_{RISC}[c] [10^6 s^{-1}]
DPAC-BPCTPA	48.9	13.8	35.1	26.3	6.2	5.25	5.49	2.73	0.57
DMAC-BPCTPA	64.6	16.2	48.4	24.5	5.3	6.61	3.62	3.06	0.75
PXZ-BPCTPA	68.9	17.3	51.6	25.2	4.2	6.87	3.10	2.97	0.95
3DPAC-BPCTPA	54.8	8.3	46.5	14.9	5.2	5.57	4.59	5.69	1.26
3DMAC-BPCTPA	74.7	11.2	63.5	13.2	5.0	8.48	2.87	6.44	1.33
3PXZ-BPCTPA	76.3	11.5	64.8	14.1	3.8	8.16	2.53	6.03	1.75

[a]Measured in doped films (20 wt% mCP films) using integrating sphere under N_2. [b]Φ_p and Φ_d are the prompt fluorescence and delayed fluorescence quantum yield, respectively; τ_p and τ_d are the lifetimes of the prompt and delayed decay components, respectively. [c]$k_{r,S}$, $k_{nr,S}$, k_{ISC} and k_{RISC} are the rate constant for fluorescence radiative transition, non-radiative transition, intersystem crossing (ISC) and reverse intersystem crossing (RISC) processes, respectively.

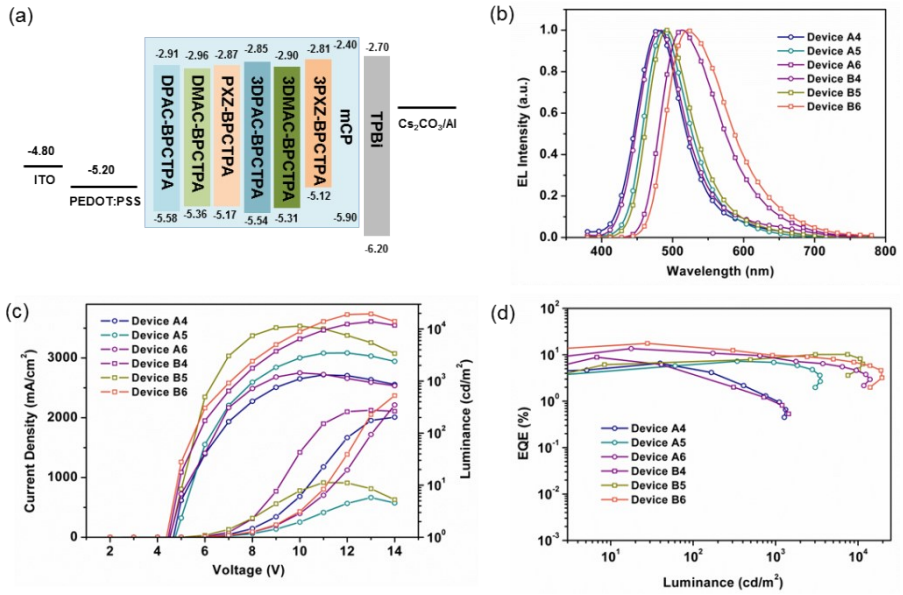

Figure S20. (a) Energy diagram of the materials used in doped devices; (b) normalized EL spectral; (c) current density-voltage-luminance (J-V-L) curves; (d) EQE versus luminance curves. Configurations: ITO/PEDOT:PSS (40 nm)/emitter (40 nm)/TPBi (30 nm) /Cs_2CO_3 (2 nm)/Al (100 nm) (Device A4: emitter = DPAC-BPCTPA (20 wt%): mCP; Device A5: emitter = DMAC-BPCTPA (20 wt%): mCP; Device A6: emitter = PXZ-BPCTPA (20 wt%): mCP; Device B4: emitter = 3DPAC-BPCTPA (20 wt%): mCP; Device B5: emitter = 3DMAC-BPCTPA (20 wt%): mCP; Device 6: emitter = 3PXZ-BPCTPA (20 wt%): mCP.

Table S6. Electroluminescence characteristics of the doped devices.

Device	λ_{em}[a] [nm]	V_{on}[b] [V]	CE_{max}[c] [Cd A^{-1}]	L_{max}[d] [cd m^{-1}]	EQE_{max}[e] [%]	PE_{max}[f] [lm W^{-1}]	CIE[g] (x,y)
Device A4	480	4.6	11.2	1323	6.6	5.9	(0.17, 0.25)
Device A5	487	4.7	16.7	3477	7.3	7.5	(0.18, 0.34)
Device A6	514	4.5	39.9	13964	13.7	25.1	(0.30, 0.54)
Device B4	483	4.4	16.8	1441	8.7	25.1	(0.18, 0.27)
Device B5	492	4.4	23.4	11393	10.2	9.2	(0.19, 0.38)
Device B6	527	4.3	52.3	19528	17.6	32.8	(0.33, 0.55)

[a]The maximum emission recorded at 6 V. [b]Turn-on voltage measured at 1 cd m^{-2}.

[c]CE_{max}= maximum current efficiency. [d]L_{max}= maximum luminance. [e]EQE_{max}= maximum external quantum efficiency. [f]PE_{max}= maximum power efficiency. [g]Commission International de I'Eclairage coordinates at 6 V.

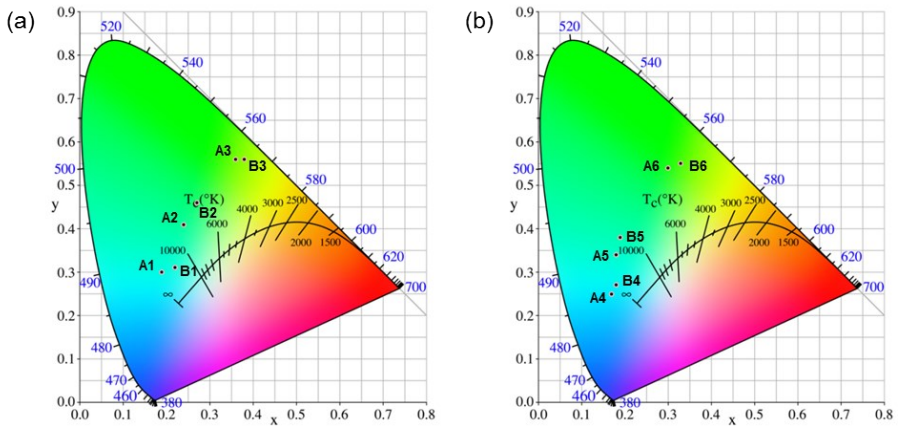

Figure S21. CIE diagram of the non-doped devices (a) and doped devices (b).

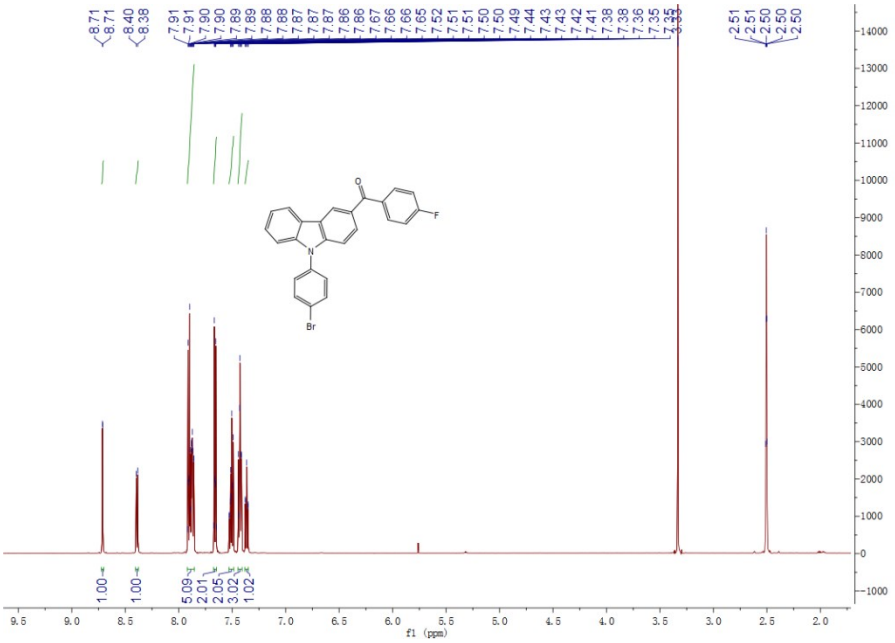

Figure S22. [1]H-NMR spectrum of 1 in DMSO-d6.

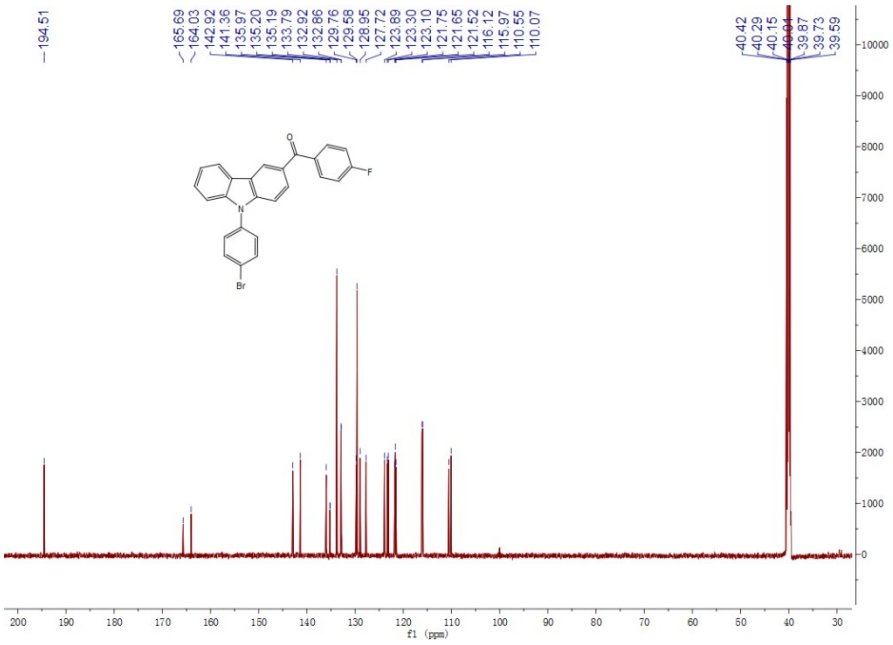

Figure S23. ^{13}C-NMR spectrum of 1 in DMSO-d6.

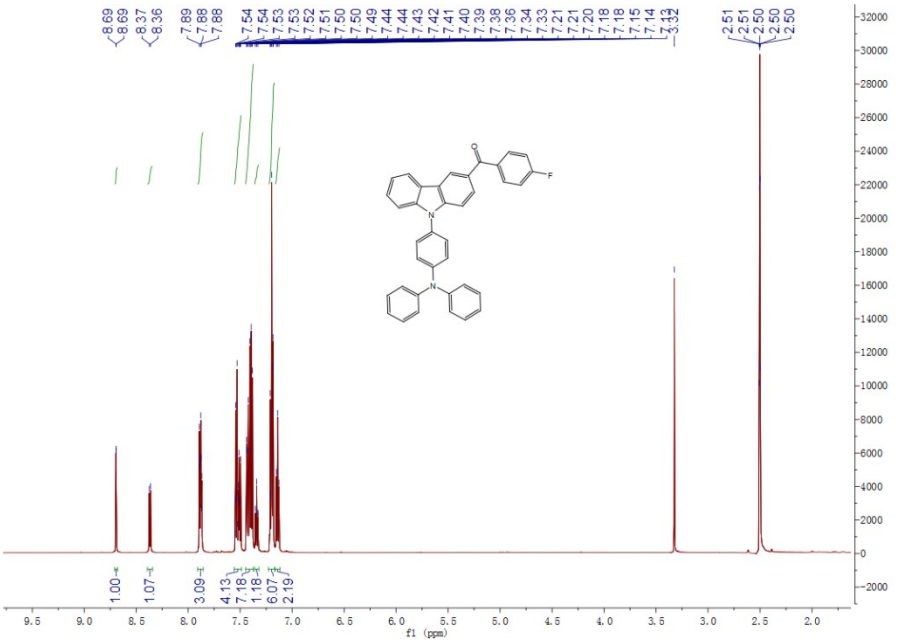

Figure S24. ^{1}H-NMR spectrum of 2 in DMSO-d6.

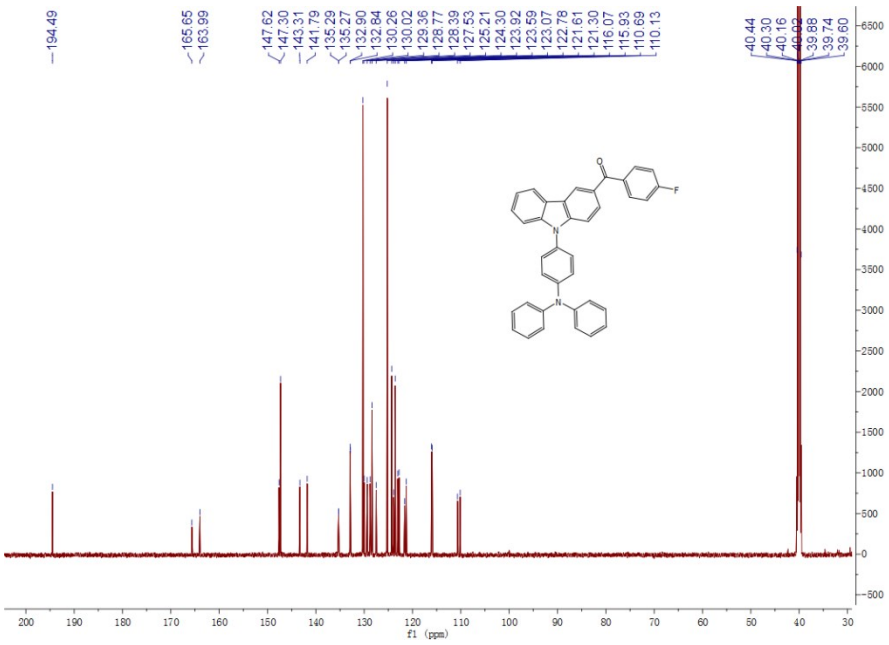

Figure S25. ^{13}C-NMR spectrum of 2 in DMSO-d6.

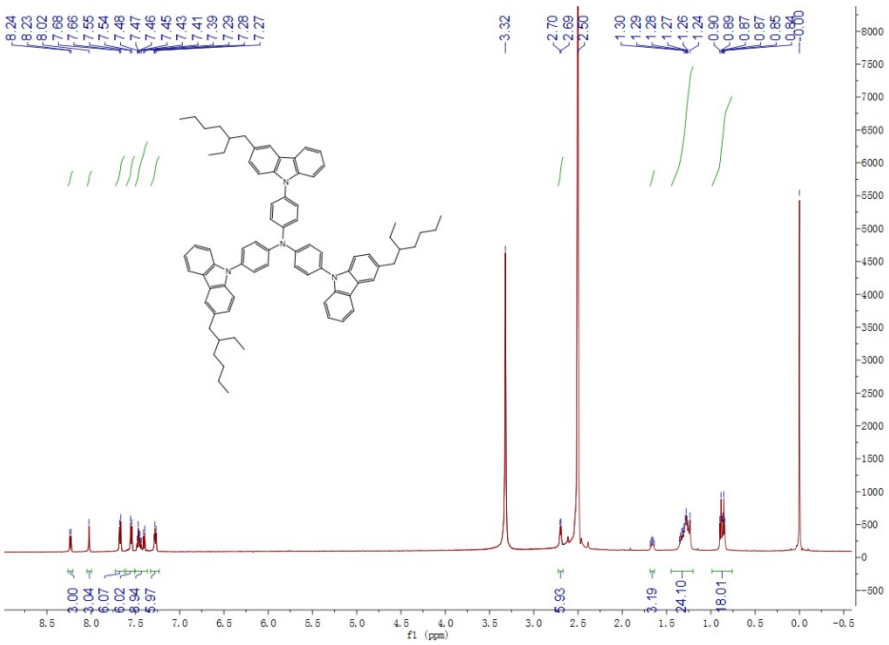

Figure S26. ^{1}H-NMR spectrum of 3 in DMSO-d6.

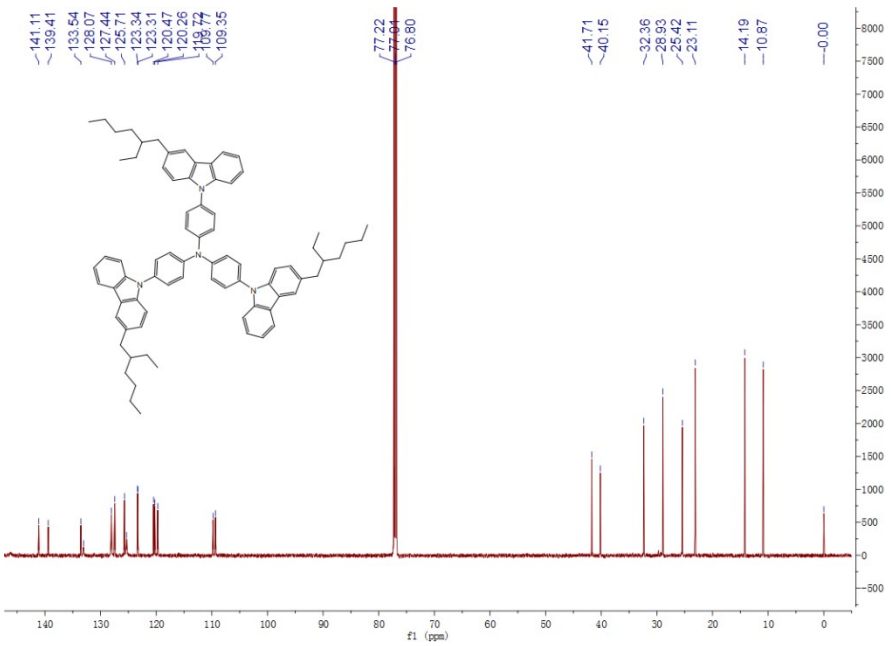

Figure S27. ^{13}C-NMR spectrum of 3 in $CDCl_3$.

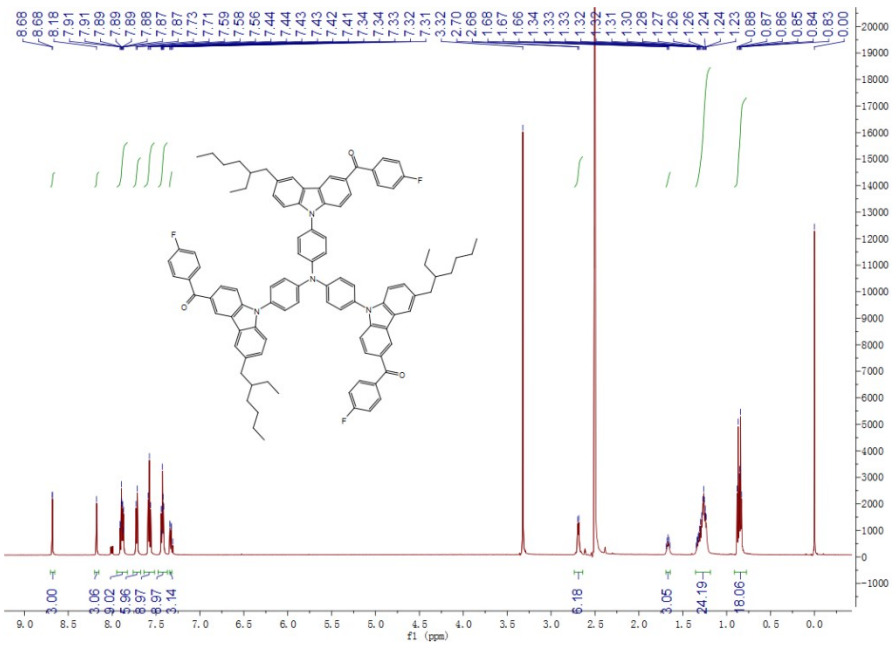

Figure S28. ^{1}H-NMR spectrum of 4 in DMSO-d6.

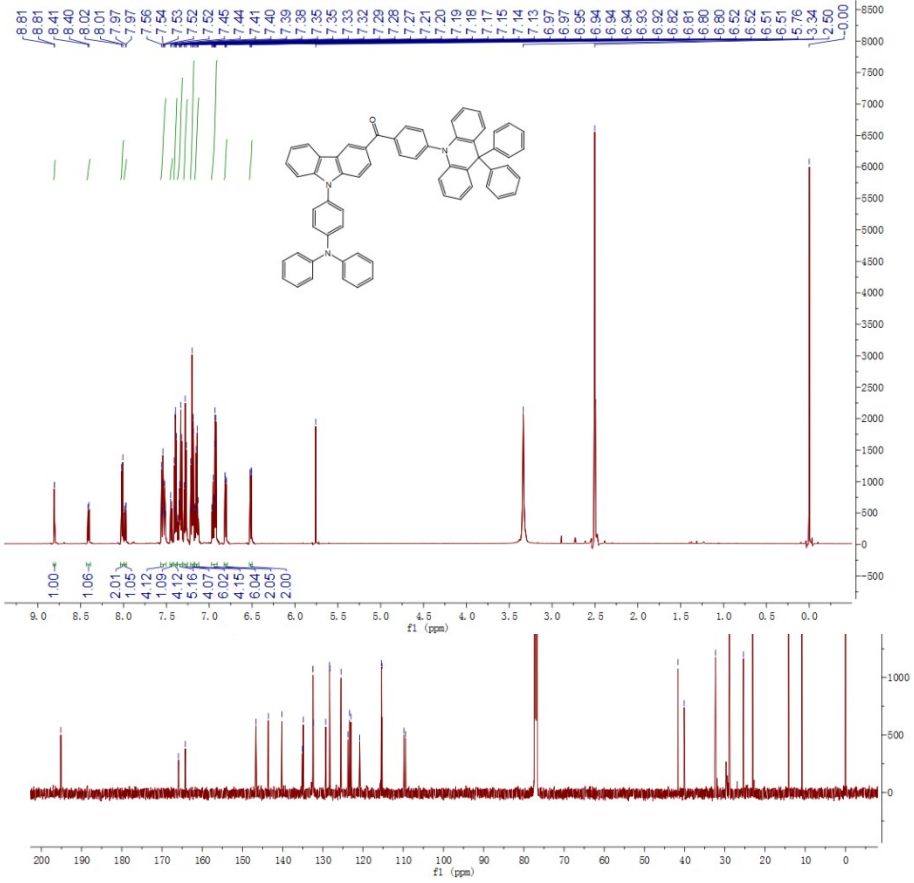

Figure S29. ^{13}C-NMR spectrum of 4 in $CDCl_3$.

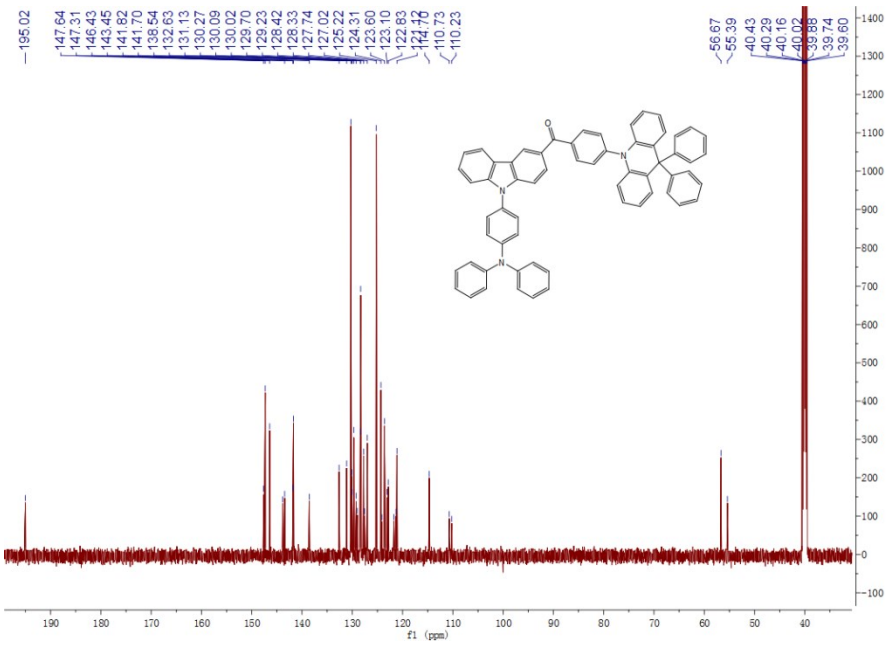

Figure S30. ^{1}H-NMR spectrum of DPAC-BPCTPA in $CDCl_3$.

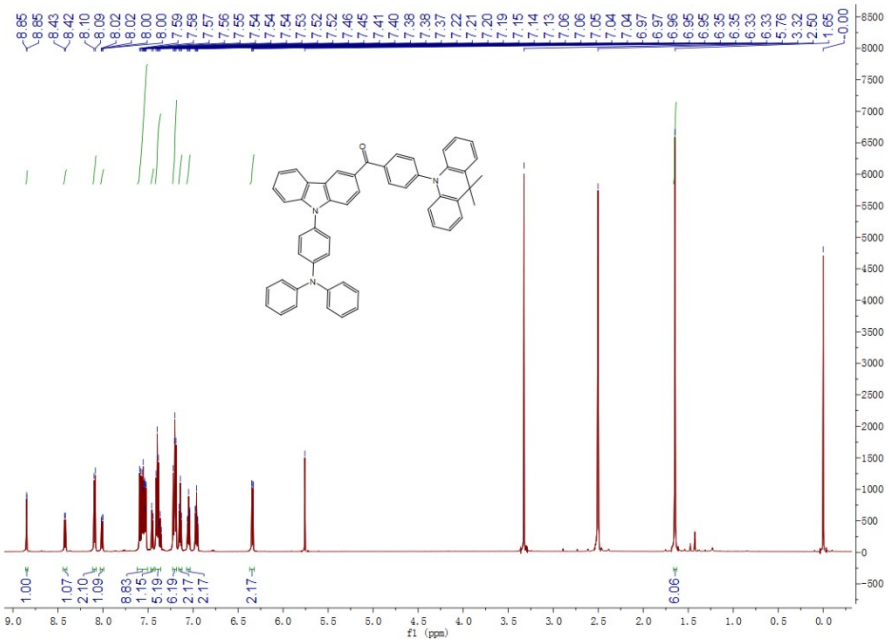

Figure S31. ^{13}C-NMR spectrum of DPAC-BPCTPA in DMSO-d6.

Figure S32. ^{1}H-NMR spectrum of DMAC-BPCTPA in DMSO-d6.

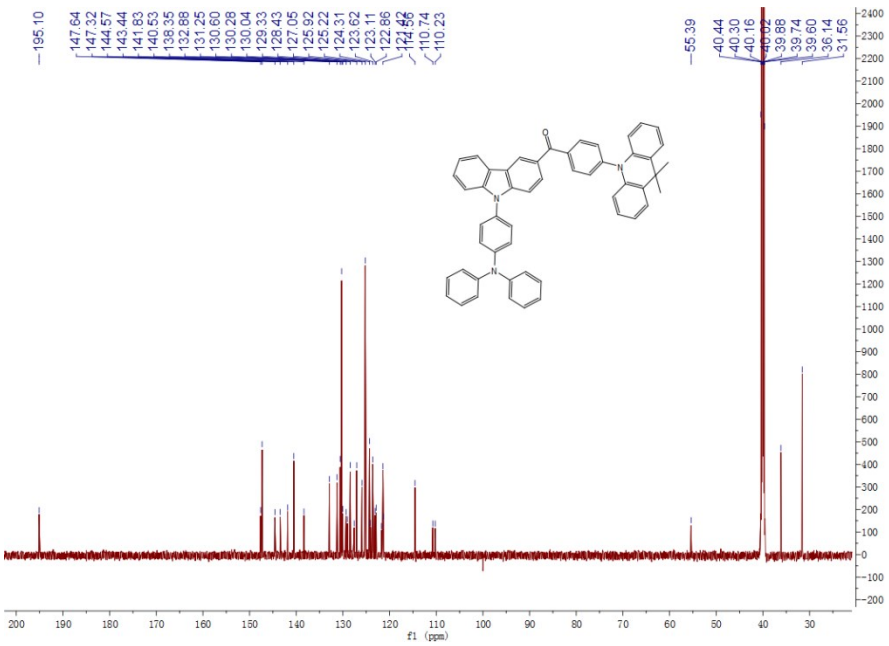

Figure S33. ^{13}C-NMR spectrum of DMAC-BPCTPA in DMSO-d6.

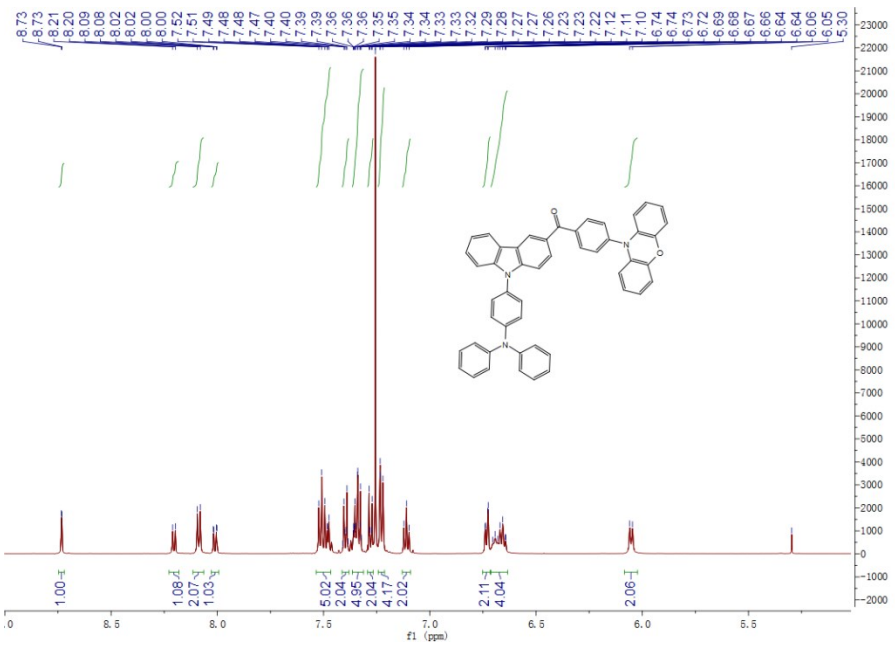

Figure S34. ^{1}H-NMR spectrum of PXZ-BPCTPA in $CDCl_3$.

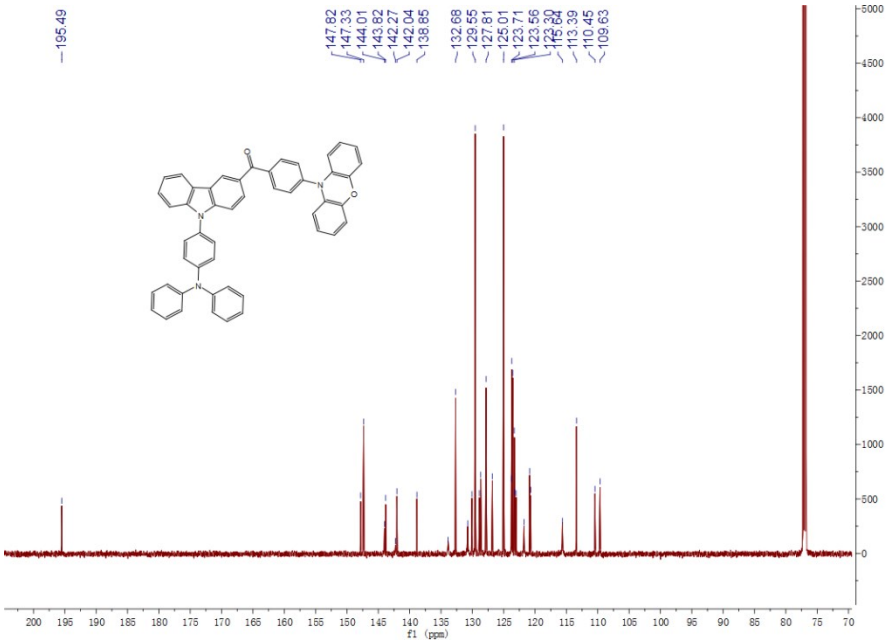

Figure S35. ^{13}C-NMR spectrum of PXZ-BPCTPA in $CDCl_3$.

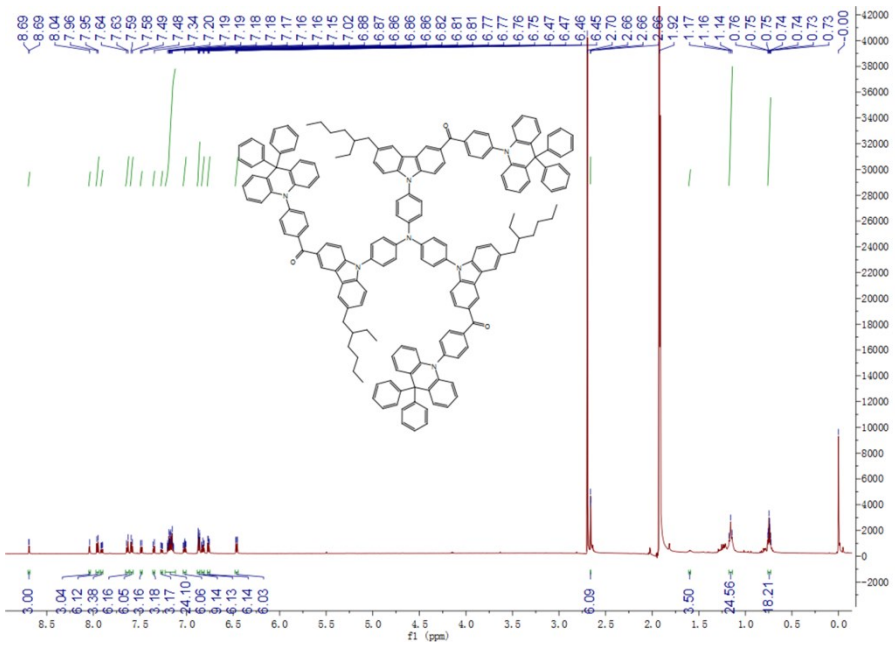

Figure S36. ^{1}H-NMR spectrum of 3DPAC-BPCTPA in Acetone-d6.

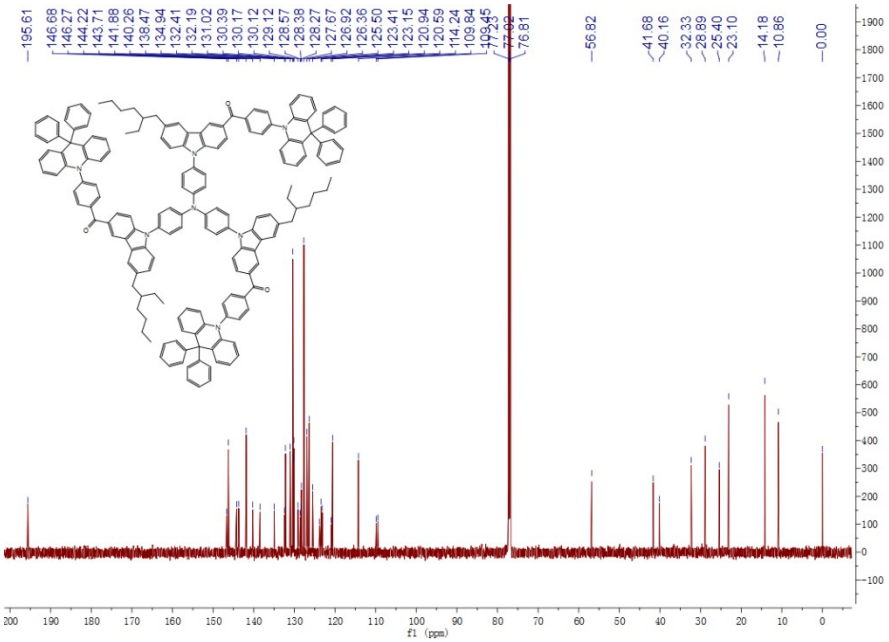

Figure S37. ^{13}C-NMR spectrum of 3DPAC-BPCTPA in $CDCl_3$.

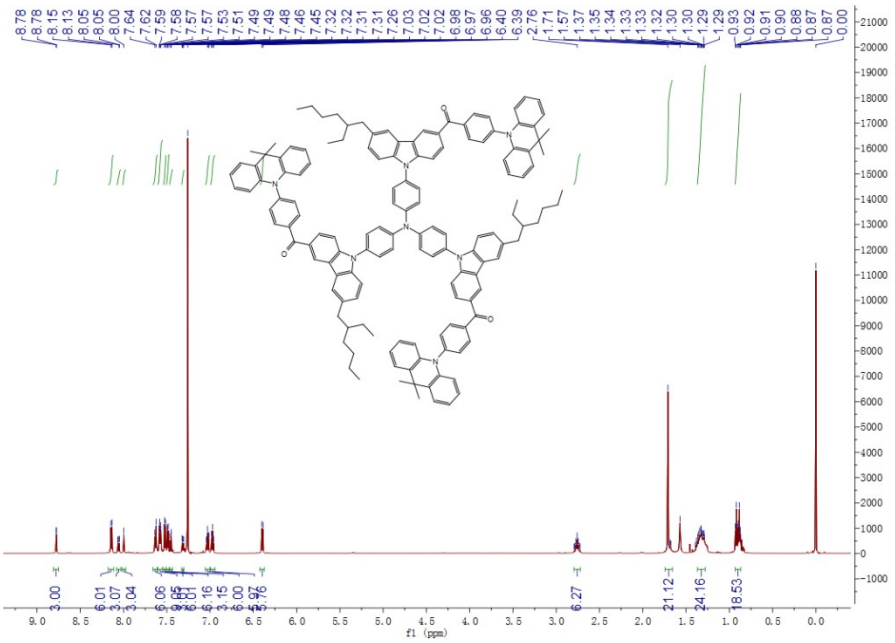

Figure S38. ^{1}H-NMR spectrum of 3DMAC-BPCTPA in $CDCl_3$.

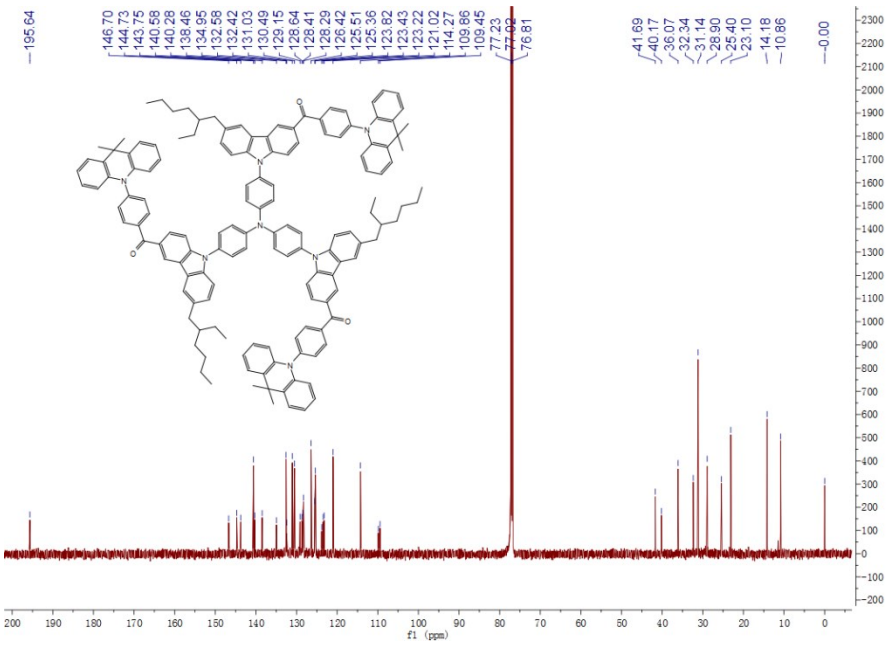

Figure S39. ^{13}C-NMR spectrum of 3DMAC-BPCTPA in $CDCl_3$.

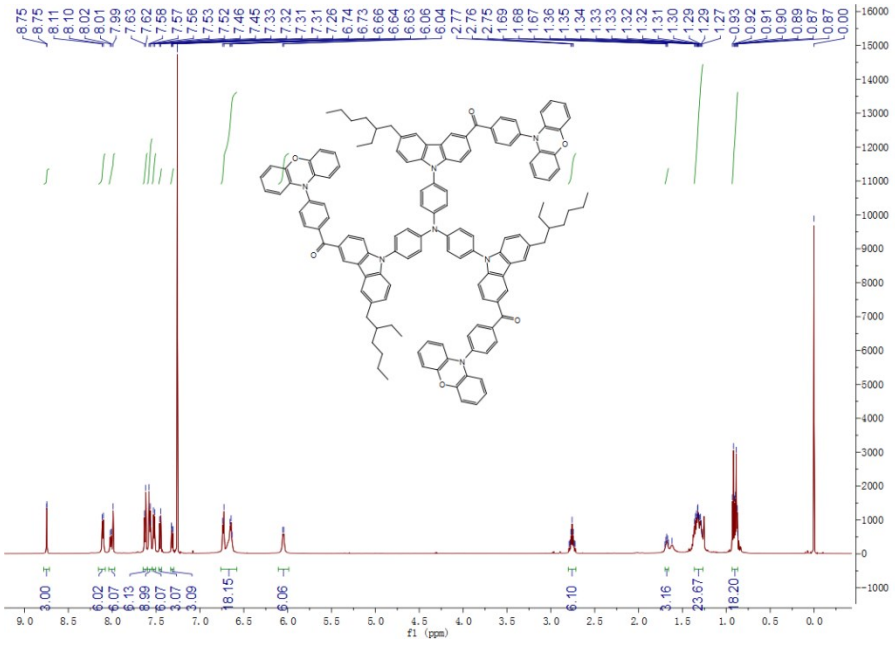

Figure S40. ^{1}H-NMR spectrum of 3PXZ-BPCTPA in $CDCl_3$.

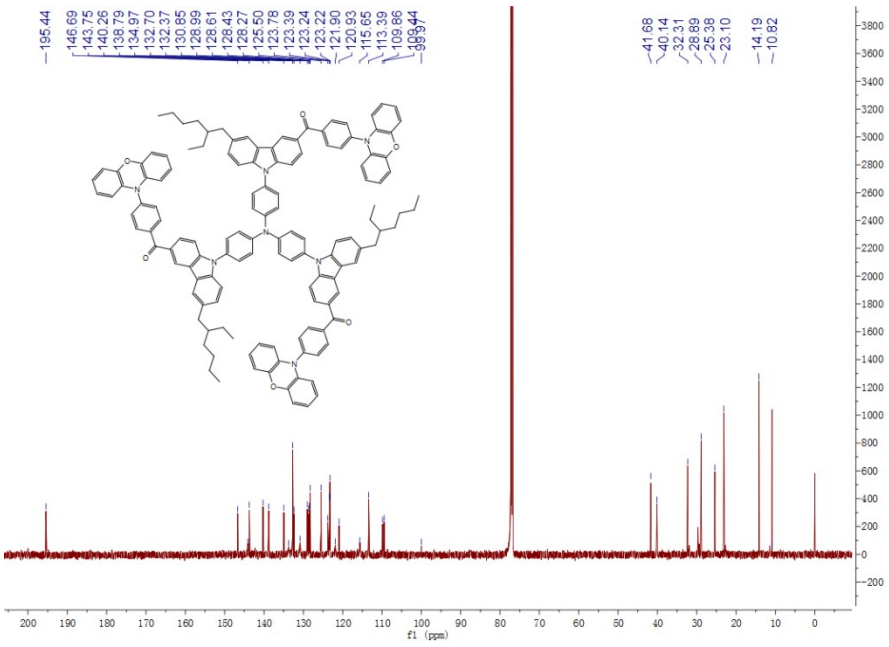

Figure S41. ^{13}C-NMR spectrum of 3PXZ-BPCTPA in $CDCl_3$.

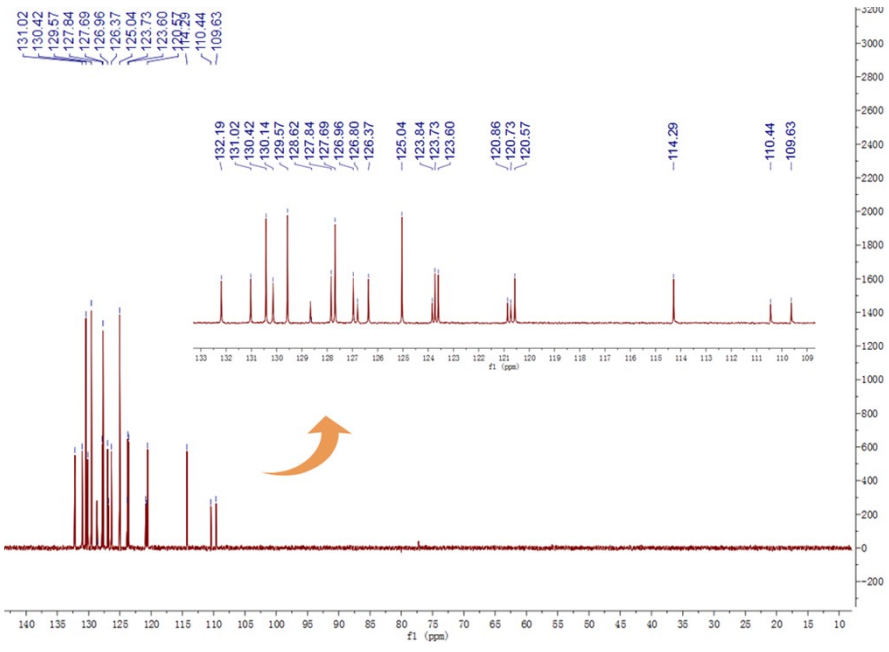

Figure S42. DEPT-135° spectrum of DPAC-BPCTPA in $CDCl_3$.

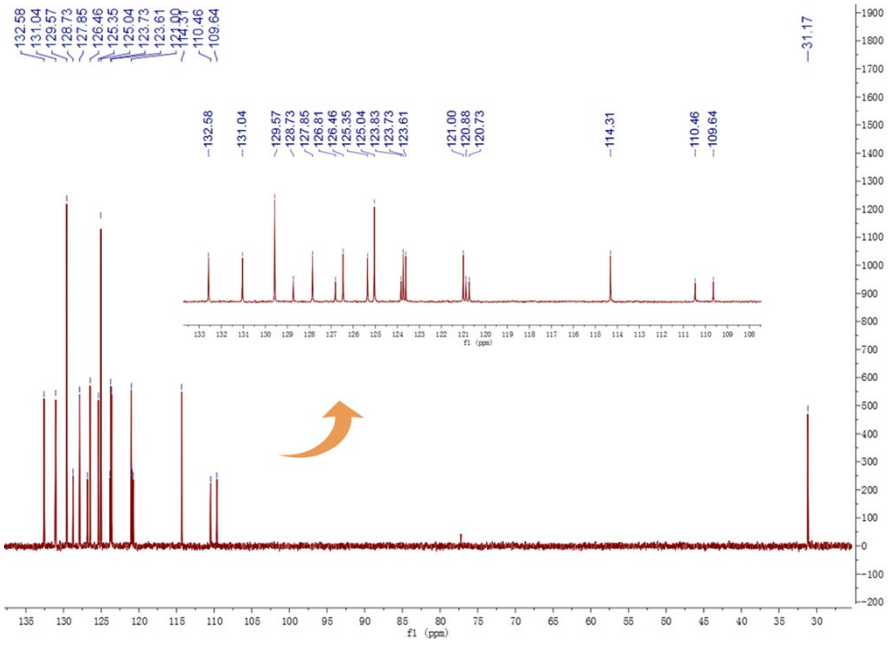

Figure S43. DEPT-135° spectrum of DMAC-BPCTPA in $CDCl_3$.

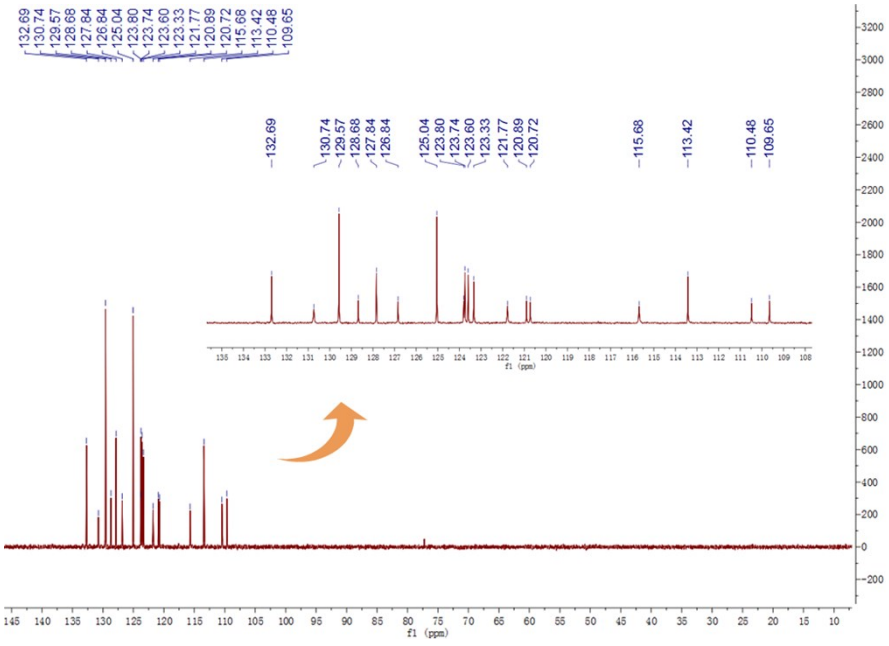

Figure S44. DEPT-135° spectrum of PXZ-BPCTPA in $CDCl_3$.

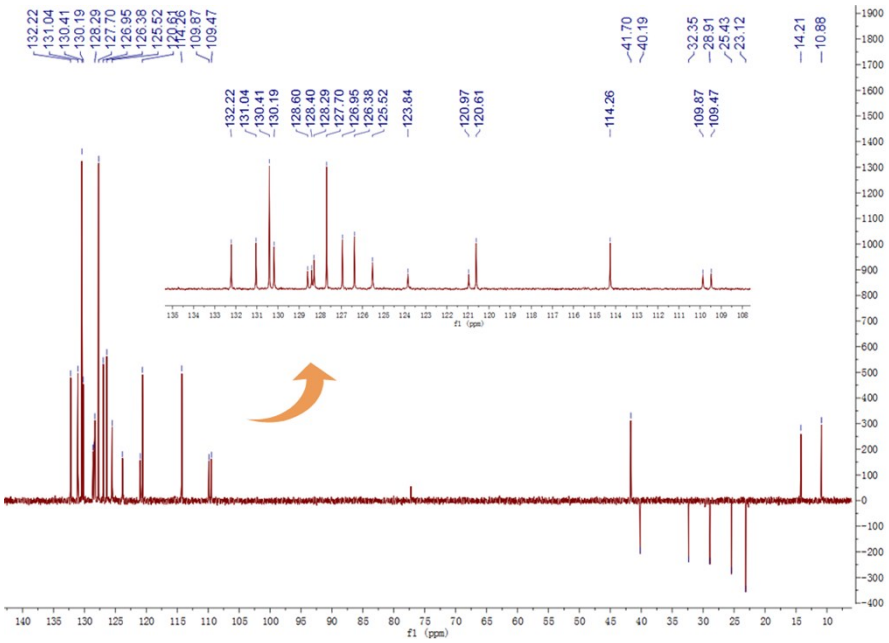

Figure S45. DEPT-135° spectrum of 3DPAC-BPCTPA in $CDCl_3$.

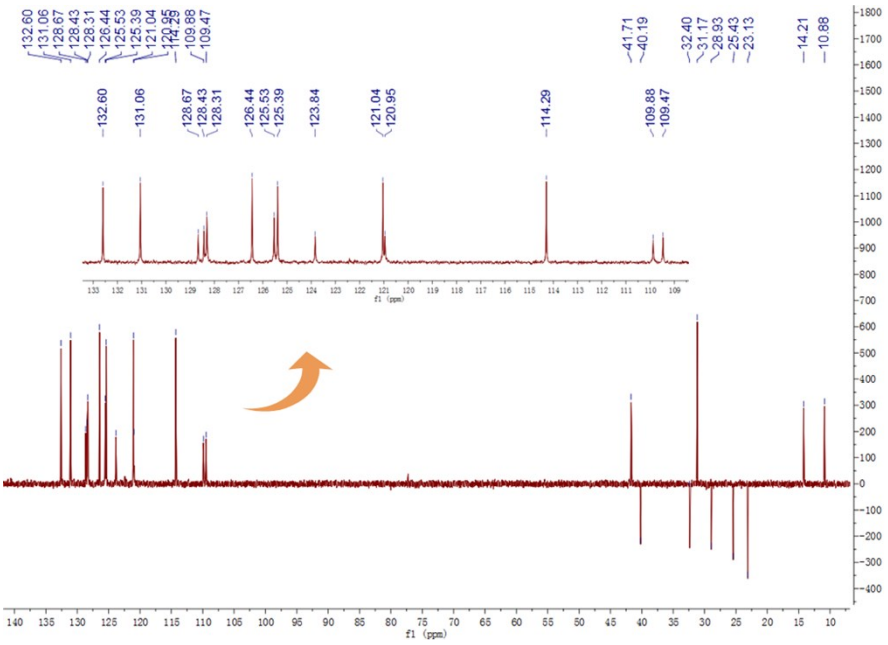

Figure S46. DEPT-135° spectrum of 3DMAC-BPCTPA in $CDCl_3$.

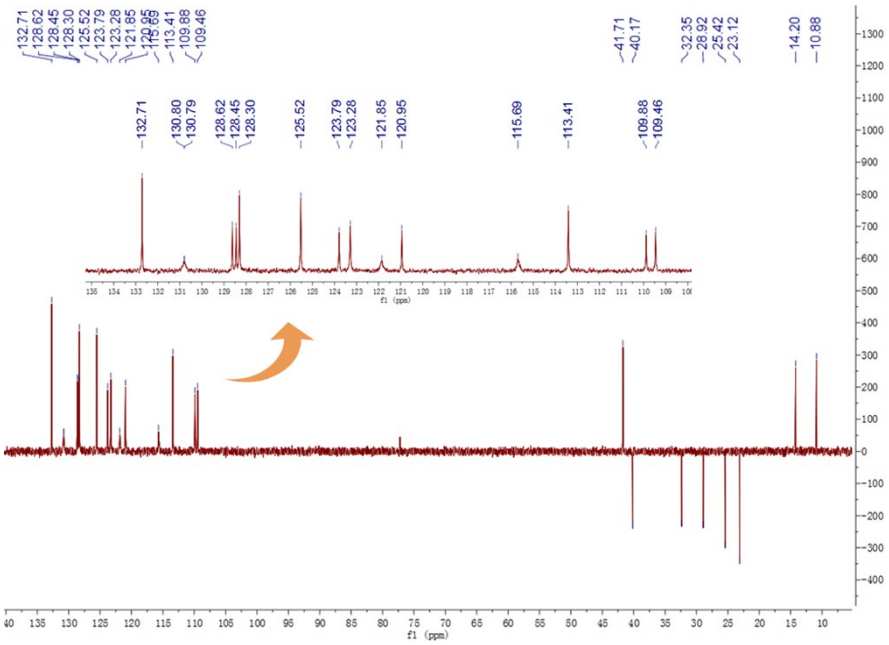

Figure S47. DEPT-135° spectrum of 3PXZ-BPCTPA in $CDCl_3$.

(1) Liu, H.; Zeng, J.; Guo, J.; Nie, H.; Zhao, Z.; Tang, B. Z. High-Performance Non-doped OLEDs with Nearly 100 % Exciton Use and Negligible Efficiency Roll-Off. *Angew. Chem., Int. Ed.* **2018,** *57*, 9290-9294.

(2) Chen, S.; Zeng, P.; Wang, W.; Wang, X.; Wu, Y.; Lin, P.; Peng, Z. Naphthalimide–Arylamine Derivatives with Aggregation Induced Delayed Fluorescence for Realizing Efficient Green to Red Electroluminescence. *J. Mater. Chem. C* **2019,** *7*, 2886-2897.